NTNU
Det skapende universitet

Mekanisk analyse av kamaksling på en skipsmotor

Steffen Sunde

NTNU – Trondheim
Norwegian University of
Science and Technology

FACULTY OF ENGINEERING SCIENCE AND TECHNOLOGY

DEPARTMENT OF ENGINEERING DESIGN AND MATERIALS

Mechanical analysis of camshaft system on a marine engine

Author:
Steffen L. SUNDE

Supervisor:
Bjørn HAUGEN

June 10, 2015

THE NORWEGIAN UNIVERSITY
OF SCIENCE AND TECHNOLOGY
DEPARTMENT OF ENGINEERING DESIGN
AND MATERIALS

MASTER THESIS SPRING 2015
FOR
STUD.TECHN. STEFFEN LOEN SUNDE

Mechanical analysis of camshaft system for a ship engine
Mekanisk analyse av kamaksling på en skipsmotor.

An increase in power for an existing ship engine will cause higher loading on the camshaft.
The project shall investigate the abilities of a current camshaft design to cope with the
increased loading.
Calculations have shown that the loading of the camshaft has significant dynamic
contributions. A review of present static calculations is therefore desired with respect to the
following effects

- Quality of present FE model and static computations
- Dynamics and backlash considerations
- Nonlinear contact effects
- Angular deflections of the transmission
- Safety factors for failure modes such as fatigue
- Vibrations and eigenfrequencies
- Tolerances
- Wear

The work will investigate how much of the engine mechanical system will have to be
integrated in a dynamic analysis in order to achieve sufficient accuracy of the transient
response for the camshaft system. When a good dynamic model has been established, this
can be used for a parameter study in order to gain insight into the important factors for a
good overall performance.
Investigating and selecting suitable analysis software and methods will be an integrated part
of the project.

Formal requirements:

Three weeks after start of the thesis work, an A3 sheet illustrating the work is to be handed
in. A template for this presentation is available on the IPM's web site under the menu
"Masteroppgave" (http://www.ntnu.no/ipm/masteroppgave). This sheet should be updated
one week before the master's thesis is submitted.

Risk assessment of experimental activities shall always be performed. Experimental work
defined in the problem description shall be planed and risk assessed up-front and within 3
weeks after receiving the problem text. Any specific experimental activities which are not
properly covered by the general risk assessment shall be particularly assessed before

performing the experimental work. Risk assessments should be signed by the supervisor and copies shall be included in the appendix of the thesis.

The thesis should include the signed problem text, and be written as a research report with summary both in English and Norwegian, conclusion, literature references, table of contents, etc. During preparation of the text, the candidate should make efforts to create a well arranged and well written report. To ease the evaluation of the thesis, it is important to cross-reference text, tables and figures. For evaluation of the work a thorough discussion of results is appreciated.

The thesis shall be submitted electronically via DAIM, NTNU's system for Digital Archiving and Submission of Master's theses.

Contact persons:
From the industry   : Håvard Solbakken, Rolls-Royce

Torgeir Welo
Head of Division

Bjørn Haugen
Professor/Supervisor

NTNU
Norges teknisk-
naturvitenskapelige universitet
Institutt for produktutvikling
og materialer

Preface

This master thesis was written at the department of Engineering Design and Materials at the Norwegian University of Science and Technology during the spring semester 2015. The report consists of a mechanical study of a medium-speed diesel engine camshaft. Special attention is paid to the dynamical behaviour during engine operation. The new B33:45 engine series from Bergen Engines AS is under development, and a study of the camshaft dynamics for different cylinder configurations is desirable. Investigating suitable analysis software and methods is an integrated part of the project.

The project is in cooperation with Bergen Engines - Rolls-Royce.

I would like to express my gratitude to the main supervisor for this project work, *Bjørn Haugen*; His knowledge and insight was crucial for the project to finish on time. I would also like to thank *Harald Berland* and *Jos van der Plas* at Bergen Engines for providing technical information and help when needed.

Steffen Loen Sunde

Trondheim, June 10, 2015

Abstract

This project is concerned with studying the dynamical behaviour of a medium-speed diesel engine camshaft. As an important part of the reciprocal engine, the camshaft is subjected to increased loading due to the growing demand of higher engine performance. The time-varying forces which acts on the camshaft in operation give rise to oscillatory motion and these vibrations are important to account for in the overall mechanical analysis.

The angular deflection of the camshaft is a key parameter in camshaft design as it affects the valve timings and hence the engine performance. The torsional vibration of camshaft is studied with special attention paid to the angular deflections. The camshaft is driven by the crankshaft through a two-stage gear drive. This gear drive has significant dynamic contributions to the camshaft performance and is included in the total model of the camshaft.

The total model is spatially discretized as a multibody system with lumped masses and interconnecting idealised springs and dampers. An integration routine was written in Matlab to simultaneously solve the equations of motion based on the Newmark β-algorithms. The nonlinearities introduced to the systems by the time-varying stiffness and backlash in the gears required an iterative solving scheme to ensure equilibrium. One of the main goal of this thesis is to develop a dynamic simulation model and investigate to which extent the different mechanical systems on the engine needs to be included in order to get a sufficiently accurate simulation model.

The dynamic response in the camshaft is found to be strongly dependent on the first natural frequency and the impulse loads introduced by the injection pumps. The results from the simulations must nonetheless be validated against physical testing before the accuracy of the model may be determined. The results were generally in concurrence with expectations and serves well as a starting point for more accurate simulation models.

Sammendrag

Dette prosjektet er et studium av den dynamiske adferden til en medium-speed diesel motor kamaksel. Kamakselen er en viktig komponent i stempelmotoren og blir utsatt for stadig høyere belastninger på grunn av økende krav til motorytelse. Den tidsvarierende belastningen under drift fører til svingende bevegelser og disse vibrasjonene er viktig å ta hensyn til i den mekaniske analysen av kamakselen.

Vinkelutslag i kamaksel er en av de viktigste parameterene i designprosessen siden den påvirker ventilstyringen og dermed også motorytelsen. Torsjonsvibrasjoner i kamaksel er studert med spesielt fokus på vinkelutslag av fri ende. På motoren er kamakselen drevet av veivakselen via en to-stegs tennhjulsdrift som viser seg å bidra med dynamiske effekter på kamakselen.

Kamakselen ble diskretisert til punktmasser med idealiserte fjærer og dempere. En integrasjonsrutine ble skrevet i Matlab for å løse systemet av differensialligninger basert på Newmarks β-metoder. Dødgang og varierende stivhet i tannhjulsdriften var blant ikke-lineære effekter som gjorde det nødvendig å implementere iterasjoner for likevekt. Et av hovedmålene i oppgaven er å utvikle en dynamisk simuleringsmodell og utforske til hvilken grad de ulike mekaniske systemene på motoren bør inkluderes for å oppnå realistiske og nøyaktige resultater. Modellen kan så brukes til videre parameterstudie.

Den dynamiske responsen i kamaksel er funnet å være dominert av den første egenfrekvensen, samt inpulslastene fra insprøytningspumpene. Resultatene som er funnet bør valideres mot fysiske målinger og tester på motor før nøyaktigheten av modellen kan bestemmes. Resultatene er forøvrig i henhold til det man på forhånd kunne forvente.

Contents

List of Figures

List of Tables

Chapter 1

Introduction

Bergen Engines AS develops medium-speed reciprocal engines for marine and power generation running on either liquid fuel or pure gas. It started out as Bergen Mekaniske Verksted (BMV) which was founded in 1855 and has since 1943 developed, manufactured and installed diesel engines for the marine industry including ferries, offshore support vessels, passenger ships and more.

Increasingly stringent environmental requirements forces engine producers to continuously improve engine design to reduce emissions but also increasing efficiency. The new B33:45 engine series from Bergen Engines is designed for efficiency and satisfies the International Maritime Organisation Tier II and tier III regulations for emissions.

The gas exchange process is important for the internal combustion engine to achieve high efficiency and low emissions and this is largely affected by the cylinder valve timings. In modern medium-speed diesel engines, including the B33:45 engine series, the cylinder exhaust and air valves are controlled mechanically by a rotating camshaft. This camshaft flexes during operation, and to have a sufficient degree of control of its motion it is necessary to study its dynamic behaviour.

1.1   Scope

The main objective of this thesis is to study the mechanical property of the camshaft design in the new B33:45 engine series. The work will investigate to which extent the different mechanical systems on the engine needs to be included in order to get a sufficiently accurate simulation model. The

simulated results should be validated against physical measurements made on the engine while on testbed. By validating and calibrating the dynamic model against measurements allows the model to be used as a parameter study on the camshaft performance.

1.2 Report outline

The underlying theory for the project is first presented in chapter 2. This includes a short introduction to the reciprocal engine and the role of the camshaft. The camshaft gear drive is regarded an important factor in the camshaft dynamic behaviour and is therefore included in the theory chapter. Mechanical vibrations and numerical methods for solving dynamic problems is outlined. A short introduction to finite element methods is also mentioned due to its importance in spatial discretization.

In chapter 3, a discrete model of the camshaft is presented.

In chapter 4, the camshaft gear drive is analysed to be added to the camshaft model. A short literature study on gear dynamics is included to summarise the common methods and assumptions.

Simulation results are presented in chapter 5, followed by a discussion of the results and finally conclusions.

The appendix section includes further simulation results and extracts of the code developed in this thesis.

1.3 Software used

Choosing suitable software is an important part of the project. To solve a complex dynamic problem, the methods and assumptions for spatial and time discretization is crucial for sufficiently accurate results to be obtained in a reasonable time frame.

MATLAB 2013b is the main tool in this project, used for numerical computations, time integration and post-processing of simulation results.

SolidWorks 2014 was used to produce three dimensional models to be studied and used as validation of results.

The finite element software suite *Abaqus 6.14* was used to assess the spatial

discretization with numerical values obtained from the models generated in SolidWorks.

FEDEM 7.1.1 was used as a validation tool.

Chapter 2

Theory

2.1 The reciprocal engine and its camshaft

The reciprocal engine converts pressure in cylinders into rotational motion through the reciprocating pistons to the crankshaft. In the diesel engine this pressure is generated by fuel which is injected into the cylinder and ignited by the temperatures generated by greatly compressing the mixture of air an fuel. Due to its high compression ratio, the diesel engine have has thermal efficiency.

2.1.1 Operating cycle

During the four stroke operating cycle, gases are exchanged through the valves in the cylinder head. As the piston moves away from the cylinder head, the air intake valves in the cylinder head are opened and air is introduced into the cylinder. The exhaust valves are closed. This is known as the *induction stroke* of the operating cycle. During the *compression stroke* all valves are closed and the piston is moved towards the cylinder head, compressing the air enclosed within the cylinder. The valves are kept closed and diesel fuel is injected into the chamber with the compressed air. The heat generated from the compression ignites the vaporised fuel particles which provides a pressure on the piston, thrusting it away from the cylinder head. This is the *power stroke*, and through the connecting rods the high pressure generated in the combustion chamber is transmitted to the crankshaft and into rotational energy. The last stroke, *exhaust stroke*, discards the exhaust gases from the combustion. The exhaust valves are opened and the piston moves towards the cylinder head again, pushing the exhaust gases through the exhaust valve

openings.

The camshaft is responsible for operating the valves and fuel injection. Rotational motion is transmitted from the crankshaft to the camshaft usually through a set of gear wheels, belt or chain. As the camshaft rotates, cam lobes distributed along its axis acts, normally on pushrod systems which in turn forces the valves to open and close. The timing of these valves and injection pumps are of critical importance for the engine to have optimal *gas exchange* which in turn affects the efficiency and emissions of the engine.

The increasingly strict emission requirements from International Maritime Organization (IMO) forces the engines to reduce NO_x and particulate emission. This makes further control of the valve timings desirable (Variable valve timing). This permits the possibility to change the timing between the exhaust valves and inlet valves and to increase their overlap.

2.1.2   Injection system

In Pump-Line-Nozzle (PLN) systems, a high pressure fuel line is responsible for the fuel injection. With the help from the camshaft the pump element generates high pressure fuel which is led to the injection nozzle to be sprayed into the combustion chamber. In newer diesel engines, the Pump-Line-Nozzle system is often replaced with *common rail*.

This master thesis is focused on the camshaft of a four stroke marine diesel engine with PLN injection system. One single camshaft is responsible for all timings, i.e. the exhaust valves, inlet valves and the fuel injection pumps.

2.2   Gears

Mechanical power is transmitted from the crankshaft to the camshaft through the gear drive. The gear drive consists of circular gear wheels with straight cut teeth of involute shape (spur gears). The involute gear tooth profile which was proposed by Leonhard Euler, is a spiral following a path traced by the end of a piece of string unwrapping from a cylinder. The involute gear profile have teeth which are involutes of a base circle. The benefits of having an involute profile is constant pressure angle, constant velocity ratio and less sensitivity to change of center distance [13].

The angle between the tooth normal and the radial line at some arbitrary point along the tooth face is called the *pressure angle*. The *pressure line* or

line of action is normal to the tooth surface and tangent to the pitch circles. See figure 2.1. The main rule of gear toothing is expressed as

$$i = \frac{\omega_1}{\omega_2} = \frac{n_1}{n_2} = \frac{d_{w2}}{d_{w1}} = \frac{z_2}{z_1} = \frac{T_2}{T_1} \tag{2.1}$$

where ω_j is the angular speed, n_j is rotational speed, d_{wj} is the pitch circle diameter, z_j is the number of teeth and T_j is the torque of the two mating gears $(j = 1, 2)$.
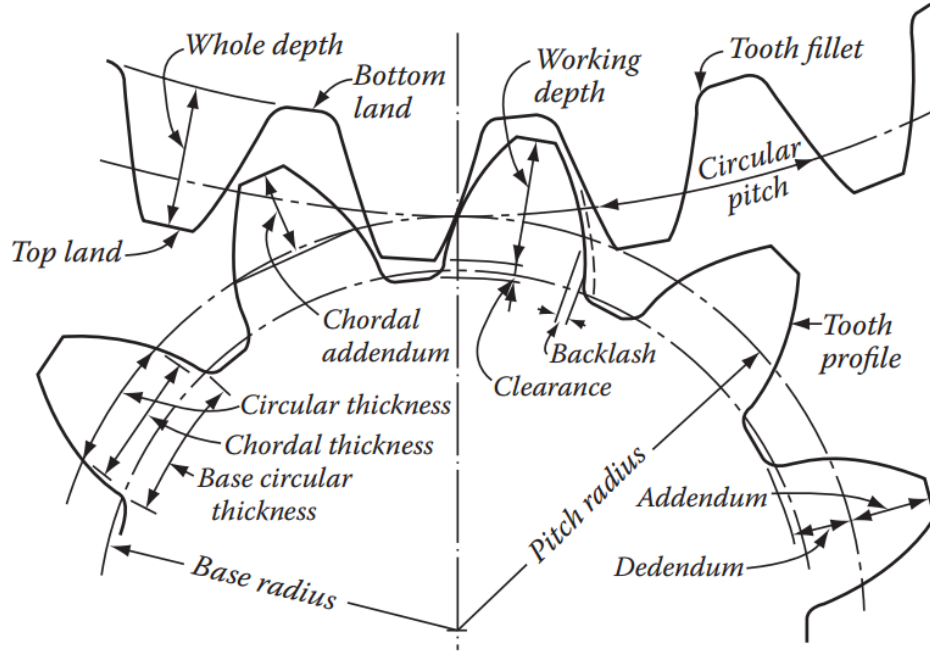
Figure 2.1: Gear nomenclature [26]

The contact ratio, CR is defined as the average number of teeth in contact during mating. Due to the risk of deformation, contact ratios should be greater than 1.2 in order not to loose contact [27]. It is important to be aware of that the theoretical values of the contact ratio are greater then the actual values.

Contact ratio can be calculated as [26],

$$m_p = \frac{\sqrt{\left(\frac{d_{ap}}{2}\right)^2 - \left(\frac{d_{bp}}{2}\right)^2} + \sqrt{\left(\frac{d_{ag}}{2}\right)^2 - \left(\frac{D_{bg}}{2}\right)^2} - C\sin\omega}{p_b} \tag{2.2}$$

where,

$$
\begin{aligned}
d_{ap},\ d_{ag} &= \text{addendum diameter of pinion and gear} \\
d_{bp},\ d_{bg} &= \text{base circle radii of pinion and gear} \\
C &= \text{operating center distance} \\
p_b &= \text{base circle pitch}
\end{aligned}
$$

High contact ratio can be achieved by increasing the number of teeth, lowering the pressure angle or increasing the addendum factor. By only increasing the addendum factor the overall configuration of the gear system will stay intact.

2.2.1   Profile shift

The choices of gear parameters are not entirely arbitrary. The choice is governed by the standardised rack cutter profiles with which the gear profile is manufactured. The tooth profile is often according to the *basic rack profile* given in the standards ISO 53 [11] or DIN 867 [6].

The position of the rack cutter may however be moved and thus shifting the involute profile inwards (negative) or outwards (positive). *Null gears* are made by having the rack cutter in nominal position, i.e. the datum line rolls over the pitch circle. The magnitude of the profile shift x is the displacement of the basic rack datum line from the reference cylinder [13].

A positive profile shift ($x > 0$) increases the tooth thickness and lowers the root bending stresses. Profile shifts are also used to achieve non-standard center distance and for avoiding undercutting in smaller gears. Negative values of x thus leads to higher bending stresses but are often chosen in gear design in order to achieve higher tooth number for a given center distance and contact ratio of the mating gears. For a given center distance between the mating gears, contact ratio and root stresses can be changed by altering the shift coefficients of the gears as long as the sum of the coefficients is held constant. This way, the gears may be optimised with respect to noise, vibration etc.

2.2.2   Tip relief

Tip relief is applied to gear teeth by removing a very small amount of material at the tips of the tooth flanks. This may be necessary to avoid the tip of the tooth to come into contact with the dedendum of the mating gear.

2.2.3 Transmission error

Deviation in real gear drives from the theoretical gears are many; shape deviations, mounting errors, etc. Transmission in loaded conditions is due to research (See section 4.1) accepted as a representative parameter for gear vibration. It is defined as the deviation from the real motion of two gears and is theoretical motion. Moreover, the *static transmission error (STE)* is this deviation under static conditions and the *dynamic transmission error (DTE)* in addition considers the inertial effects.

In dynamic gear models, the transmission error $e(t)$ is often modelled as a periodic displacement excitation along the pressure line of the gears and with period given by the *fundamental meshing frequency* of the gear given by

$$\Omega = z_p \Omega_p \tag{2.3}$$

where z_p is the number of teeth and Ω_p is the rotational frequency of the pinion.

2.2.4 Gear backlash

In theoretical gears the tooth thickness of a gear matches the space width of the mating gear. The working and non-working tooth faces mesh at the same time. In real gear drives however, there will be a small gap between the flanks of the mating gears, known as *backlash*. See figure 2.1. Backlash is often included by tolerances in the machining process and does not affect the nominal dimensions of the gears. Backlash may also be introduced to the gear pair by slightly increasing the center distance. Backlash is essential for correct lubrication and to prevent the gears from jamming.

High temperature differences in the operating conditions for modern diesel engines increases the need for backlash to allow for thermal expansion.

In an oscillating system however, backlash may lead to loss of contact of the mating gear teeth, which in turn can introduce high dynamic loads to the system. This dynamic effect is often called *gear hammering*.

2.3 Mechanical vibrations

Dynamics is the study of the motion of physical bodies and the forces acting upon them. An important part of dynamics is mechanical vibrations which is the oscillatory motion around stable equilibrium. To simulate the mechanical vibrations of a real system, an idealised mathematical model is constructed to represent the real system with acceptable degree of accuracy. A continuous problem is approximated in a discrete model with a finite number of *degrees of freedom (DOFs)*, mathematically described by a set of ordinary differential equations (ODE) which is well suited for computer implementation. The continuous system having infinite number of degrees of freedom can be viewed as the limiting case for the discrete model, whose accuracy can be improved by increasing the number of DOFs.

2.3.1 Euler-Lagrange

The principle of *virtual work* states that a system is in equilibrium if and only if the total virtual work of the applied forces is zero. This leads to the *d'Alembert principle* which can be rewritten to the *Lagrange equations (LE)* [7]. The Lagrange equations describes a system of m degrees of freedom with m *generalised coordinates*. The generalised coordinates can be cartesian coordinates, angles or whatever is convenient for the actual problem. The motion of a system can in Lagrangian mechanics be described using the Euler-Lagrange equation

$$\frac{d}{dt}\left(\frac{\partial L}{\partial \dot{q}_j}\right) - \frac{\partial L}{\partial q_j} = Q_j \tag{2.4}$$

where $j = 1, 2, ...m$ represents the jth degree of freedom, q_j are the generalised coordinates and $\dot{q}_j$ are the generalised velocities. Q_j is the generalised force that add energy to the system. The dynamics of the system is summarised in the *Lagrangian L* of the system and is defined as the difference between its *kinetic energy T* and *potential energy V*.

$$L = T - V \tag{2.5}$$

The equations of motion can thus be obtained for a system if the Lagrangian 2.5 of the system is known. In mechanical vibration frequently encountered forces are *elastic* forces and *viscous* forces. The elastic strain forces are in the Lagrangian accounted for in as a potential energy term. The Euler-Lagrange

equation (2.4 can be extended to account for non-conservative forces like viscous friction by including a *dissipation function D*.

$$\frac{d}{dt}\left(\frac{\partial L}{\partial \dot{q}_j}\right) - \frac{\partial L}{\partial q_j} + \frac{\partial D}{\partial \dot{q}_j} = Q_j \tag{2.6}$$

which for the linear case leads to the equations of motion [7]

$$\sum_j \left(m_{rj}\ddot{u}_j + c_{rj}\dot{u}_j + k_{rj}u_j\right) = 0 \quad (r = 1, ...n) \tag{2.7}$$

Including the generalised forces and expressing the equations of motion in matrix form gives

$$\boldsymbol{M}\ddot{\boldsymbol{u}} + \boldsymbol{C}\dot{\boldsymbol{u}} + \boldsymbol{K}\boldsymbol{u} = \boldsymbol{f} \tag{2.8}$$

where $\boldsymbol{M}$, $\boldsymbol{C}$ and $\boldsymbol{K}$ are nxn matrices with the inertia-, damping- and stiffness coefficients respectively.

2.3.2   Nonlinear dynamics

In the case of nonlinear dynamics, the equations of motion may be expressed as [8]

$$\boldsymbol{M}\ddot{\boldsymbol{u}} + \boldsymbol{f}(\boldsymbol{u}, \dot{\boldsymbol{u}}) = \boldsymbol{g}(\dot{\boldsymbol{u}}, t) = Q_j \tag{2.9}$$

where $\boldsymbol{f}(\boldsymbol{u}, \dot{\boldsymbol{u}})$ represents the internal forces as functions of the displacements and velocities which includes both elastic and internal dissipative forces. $\boldsymbol{g}(\dot{\boldsymbol{u}}, t)$ is the vector of external forces.

Matrix notation will be used throughout this thesis. It is regarded as convenient due to it being compact in notation and it is easy to implement in computer code as two-dimensional arrays.

2.3.3   Free vibration

By setting the force vector in equation 2.8 to zero, the problem is reduced to one of *free vibration*. In the absence of dissipative forces ($\boldsymbol{C} = 0$), a system

with an initial disturbance from its equilibrium position will oscillate forever, unless disturbed again. This motion is called *undamped free vibration* and can be analysed by assuming that the solution for $\boldsymbol{u}$ is on the form

$$\boldsymbol{u}(t) = \boldsymbol{z}e^{-i\omega t} \tag{2.10}$$

where $\boldsymbol{z}$ is the *shape vector* and ω is the corresponding *natural frequency*. By inserting into the free vibration equation and rewriting to *standard eigenvalue problem* form one obtains

$$\left(\boldsymbol{K} - \omega^2 \boldsymbol{M}\right)\boldsymbol{z} = 0 \tag{2.11}$$

For a system of n degrees of freedom solving the eigenvalue problems means finding the *eigenvectors* $\boldsymbol{z}$ and its corresponding *eigenvalues* ω^2 one for each degree of freedom. Physically, the values of the eigenvalues $\omega_1, \omega_2, ..., \omega_n$, represents the natural frequencies of the system, with the lowest, ω_1, called the *fundamental frequency*. The corresponding eigenvectors $\boldsymbol{z}_1, \boldsymbol{z}_2, ..., \boldsymbol{z}_n$, each represents a *mode* of vibration. Owing to the linearity of the system, the solution to the undamped free vibration can be expressed as

$$\boldsymbol{u} = \sum_{j=1}^{n} \left(A_j e^{i\omega_j t} + B_j e^{-\omega_j t}\right) \boldsymbol{z}_j \tag{2.12}$$

where the constants A and B are obtained by using the initial conditions. This method for solving the dynamic equations is known as modal superposition technique and is very efficient for solving systems with a limited number of DOFs and which are dominated by the lowest modes. This technique is also clearly limited to the linear case. Problems in which a higher number of modes needs to be accounted for, and for nonlinear problems, modal superpositioning should be replaced with *direct time integration methods* [8]

By including the damping term of the equation 2.8, the eigenvalue problem becomes *complex* and the free vibration of the damped system is no longer synchronous, i.e. each degree of freedom is not necessarily in phase.

2.4   Finite element method

Finite element software is used to assess the method of spatially discretizing the problem. The finite element method (FEM) is a numerical technique

for solving field problems like stress distribution, fluid flow, thermal fields etc. By dividing the subject of interest into a finite number of elements, the problem is discretized to a boundary value problem with a set of equations to be solved for each element. These equations are then systematically put together and solved numerically. Because of this discretization, finite element calculations will only provide an approximate solution, but the solution is generally increasingly accurate with increasing number of elements - at the cost of more equations to solve.

In structural analysis, the *direct stiffness method* is the most common technique for solving structural problems with the finite element method. The body of interest is separated into smaller idealized elements with interconnecting and shared nodes. Stiffness is found for each element and gathered in a stiffness matrix. This matrix is solved for the structure's unknown displacements at the nodes by matrix operations. This numerical method for solving a system of equations may be an extremely time consuming process, but is well suited for computer processors [17].

For three dimensional structures, solving the governing differential equations analytically is difficult if not impossible. But by using weighted residual methods, the solutions is replaced with approximate algebraic equations. The governing system equations are partial differential equations of strong form which is difficult to solve for practical engineering problems because of continuity requirements. However, by applying a finite sum of test functions, the solution is well approximated and the continuity requirement is lowered.

The nodal displacements are interpolated locally over each element using shape functions. As an illustration, consider the two dimensional quadrilateral element and its shape functions:

$$
\begin{aligned}
N_1(\xi, \eta) &= \frac{1}{4}(1 - \xi - \eta + \xi\eta) \\
N_2(\xi, \eta) &= \frac{1}{4}(1 + \xi - \eta - \xi\eta) \\
N_3(\xi, \eta) &= \frac{1}{4}(1 + \xi + \eta + \xi\eta) \\
N_1(\xi, \eta) &= \frac{1}{4}(1 - \xi + \eta - \xi\eta)
\end{aligned}
\tag{2.13}
$$

2.4.1 Element types

There are a number of different element types and the best element of choice is often depending on the problem to be solved. The most simple element

is the one dimensional *truss* element with two nodes, one in each end. The truss element is only subjected to axial loads and no bending. For the one dimensional beam element on the other hand, the end nodes inhibits a rotational degree of freedom and therefore may have shear forces and moments. One dimensional elements will often for simple problems serve as a first hand calculation, but most three dimensional problems calls for more sophisticated methods. Most FEM software today including Abaqus offers a set of tools for generating an element mesh of the problem of interest. It is however important for the user to have knowledge to element behaviour to be able to evaluate the solutions.

Displacements are calculated at the nodes and interpolated over the element. The degree of the shape functions for the interpolation is determined by the number of the nodes. Elements only having nodes at the corners will have their displacement vary linearly along the edges. These elements are therefore called linear elements or first-order elements. Linear elements often give reasonably accurate results, but are somewhat coarse due to the linearity and should therefore be avoided in areas with high gradients [29].

Higher order elements have added nodes at the element sides, and thus the polynomial degree of the shape functions increases. Quadratic elements are of second order and have one additional node at the edges. Quadratic elements clearly gives a more accurate shape of the element and the total number of elements may therefore be lowered compared to having linear elements.

2.5   Numerical methods

Unlike for the single degree of freedom (SDOF) oscillator, most ordinary differential equations cannot be solved analytically. Even if they can, in many cases a numerical method for obtaining a solution (or several) is more appropriate.

As the continuous problem is discretized in the spatial domain to a set of differential equations, numerical integration methods are used to discretized the problem in the time domain. The continuous model is approximated in that the solutions are only found for discrete points in time.

Knowledge to the methods of numerical solving of differential equations is important in order to use the appropriate algorithms and for interpreting the results. The choice of algorithm is related to the *stability*, *accuracy*, *computational costs* etc. Of importance is also the distinction between linear and non-linear differential equations.

The generic form of the first order differential equation with an initial condition can be

$$\frac{df(x)}{dx} = G(x) \, f(a) = f_a \tag{2.14}$$

where x is an independent variable like time and position and t is a function of this independent variable and $f(x)$ is a given function of x. If analytical integration is not applicable, numerical integration may be, with the goal of generating a set of approximate solutions to $f(x)$ at equally spaced positions along the ODE. A function $f(x)$ satisfying certain conditions about a point $x = a$ can be given by the Taylor series expansion given by

$$f(x) = f(a) + f'(a)(x-a) + \frac{f''(a)}{2!}(x-a)^2 +$$

$$... + \frac{f^{(n)}(a)}{n!}(x-a)^n + ... \tag{2.15}$$

$$= \sum_{n=0}^{\infty} \frac{f^{(n)}(a)}{n!}(x-a)^n$$

which means that the function at some point can be approximated by the the function value at a nearby known point and its known derivatives as

$$f(t + \Delta t) = f(t) + \Delta x f'(t) + \frac{1}{2}\Delta t^2 f''(t) + O(\Delta t^3) \tag{2.16}$$

for small values of δt. The remainder, $O(\Delta t)$ represents the higher order terms which are omitted, called *big O* in *Landau notation*. Also called the local truncation error for the specific step, $O(h^{p+1})$ means that the numerical method has the order p. The *global truncation error* is the accumulated local truncation error over the integration process. The numerical method is said to *converge* if the global truncation error approaches zero as the step size Δx goes to zero.

One of the key concepts of numerical solutions is the combination of function values at different points to approximate the derivatives. Direct integration methods can in the general form be expressed as

$$\boldsymbol{u}_{n+1} = \sum_{i=1}^{m} \alpha_i \boldsymbol{u}_{n+1-i} - h \sum_{i=0}^{m} \beta_j \dot{\boldsymbol{u}}_{n+1-i} \tag{2.17}$$

where $h = t_{n+1} - t_n$ is the time step and where $\boldsymbol{u}_{n+1}^T = [\dot{\boldsymbol{u}}_{n+1}^T \boldsymbol{u}_{n+1}^T]$ is the solution or state vector at time t_{n+1} calculated from the state vectors from the m preceding time steps.

For $\beta_0 \neq 0$, the integration method is said to be *implicit* since the solution of the state vector is a function of it's own derivative. Implicit methods thus needs to be solved as a system of equations. Methods in which $\beta_0 = 0$ are *explicit* and the solution of each time step is given directly from the previous time steps.

When α_i and β_i are all zero for $i > 1$, the equation 2.17 is said to be a single-step integration method and the time steps are thus calculated based upon only the previous state vector.

2.5.1 Explicit methods

One of the simplest integration formulas is the *Eulers's method*, which is obtained from 2.17 by setting $\alpha_1 = 1$ and $\beta_1 = 1$ which is a single step explicit method with global truncation error $O(h)$. Accuracy can be improved, however, by including more terms from the Taylor series 2.15. Euler's method is the simplest of the *Runge-Kutta* family of iterative methods. Higher order of Runge-Kutta methods are often used in structural dynamics problems, most often the fourth (RK4) or fifth order (RK5) [10].

In structural dynamics, nonlinear problems are often solved with explicit time integration schemes. The explicit methods are easy to implement but often require very small time steps to ensure stability. If the structure has high-frequency modes, the time step will have to be small and the total number of steps is needed for the time history analysis. This makes explicit methods especially appropriate for *wave propagation problems* like shock response or impact where the high-frequency modes are important.

Stability restriction in explicit methods was discussed by Courant et. al. in 1928 [25]. They introduced the *courant number r* by

$$r = \frac{c \Delta t}{\Delta x} \qquad (2.18)$$

where c is the wave propagation speed and Δx is the length of the element. The Courant-Friedrichs-Lewy (CFL) condition is $r \leq 1$ which can be interpreted as: Rate of numerical information flow must be equal to or greater than the rate of information flow in the continuous problem. The CFL critera is a necessary condition for stability but not necessarily sufficient. This implies that the smallest element in the structure dictates the step

size for the whole structure. It is not uncommon, however, to use "hybrid" methods which permits the use of both implicit and explicit methods to be used simultaneously in different parts of the model. This was demonstrated for transient dynamic problems by Liu and Belytschko [20].

2.5.2 Implicit methods

The implicit method proposed by Nathan M. Newmark in his 1959 paper [23] The Newmark family of methods are some of the most popular methods for direct time integration. The solution at time step t_{n+1} is achieved through a Taylor expansion series of the displacements and velocities of the previous time step t_n. The Newmark method is thus a single-step method.

The linear dynamic equation (2.8) serves well for demonstrating Newmark's method. The velocities and accelerations of the structure in the next point in the time marching process $n + 1$ is given by the Taylor expansion series (equation 2.15).

$$
\dot{\boldsymbol{u}}_{n+1} = \dot{\boldsymbol{u}}_n + \int_{t_n}^{t_{n+1}} \ddot{\boldsymbol{u}}(\tau)\,d\tau
$$

$$
\boldsymbol{u}_{n+1} = \boldsymbol{u}_n + h\dot{\boldsymbol{u}}_n + \int_{t_n}^{t_{n+1}} (t_{n+1} - \tau)\dddot{\boldsymbol{q}}(\tau)\,d\tau
$$

(2.19)

Newmark approximated the integral terms and introduced the two parameters γ and β which enables the direct time integration method to be adjusted for accuracy and stability. By inserting

$$
\int_{t_n}^{t_{n+1}} \ddot{\boldsymbol{u}}(\tau)\,d\tau = (1 - \gamma)h\ddot{\boldsymbol{u}}_n + \gamma h\ddot{\boldsymbol{u}}_{n+1} + O(h^2\boldsymbol{u}^{(3)})
$$

$$
\int_{t_n}^{t_{n+1}} (t_{n+1} - \tau)\ddot{\boldsymbol{u}}(\tau)\,d\tau = \left(\frac{1}{2} - \beta\right)h^2\ddot{\boldsymbol{u}}_n + \beta h^2\ddot{\boldsymbol{u}}_{n+1} + O(h^3\boldsymbol{u}^{(4)})
$$

(2.20)

into equation 2.19 the Newmark method can be expressed as

$$\dot{\boldsymbol{u}}_{n+1} = \dot{\boldsymbol{u}}_n + (1-\gamma)h\ddot{\boldsymbol{u}}_n + \gamma h\ddot{\boldsymbol{u}}_{n+1}$$

$$\boldsymbol{u}_{n+1} = \boldsymbol{u}_n + h\dot{\boldsymbol{u}}_n + h^2\left(\frac{1}{2}-\beta\right)\ddot{\boldsymbol{u}}_n + h^2\beta\ddot{\boldsymbol{u}}_{n+1}$$

(2.21)

Applying the marching scheme of Newmark to equation 2.8 results in the dynamic equilibrium at time t_{n+1} as a function of the acceleration vector $\ddot{\boldsymbol{u}}$:

$$\left[\boldsymbol{M} + \gamma h\boldsymbol{C} + \beta h^2 \boldsymbol{K}\right]\ddot{\boldsymbol{u}}_{n+1} = \boldsymbol{F}_{n+1} - \boldsymbol{C}\left[\dot{\boldsymbol{u}} + (1-\gamma)h\ddot{\boldsymbol{u}}_n\right]$$
$$- \boldsymbol{K}\left[\dot{\boldsymbol{q}}_n + h\dot{\boldsymbol{u}}_n + \left(\frac{1}{2}-\beta\right)h^2\ddot{\boldsymbol{q}}_n\right]$$

(2.22)

from which the acceleration vector $\ddot{\boldsymbol{u}}_{n+1}$ may be calculated. The velocity vector and position vector can then be calculated from equation 2.21. The scheme is illustrated in figure 2.2. Note that if the time stepping length h is held constant, the iteration matrix $\boldsymbol{N}$ will only have to be inverted once. This makes it a very fast algorithm for linear systems.

The two constants β and γ can be chosen for different quadrature schemes. *Average acceleration scheme* is obtained by setting

$$\gamma = \frac{1}{2} \qquad \beta = \frac{1}{4}$$

(2.23)

in which acceleration is assumed to be constant over the time step. It can be shown that for the undamped case, the average acceleration scheme is most accurate *unconditionally stable method* [8]. Unconditional stability means that there are no limitations to the time step.

By setting $\gamma = 1/2$ and $\beta = 0$ the *central difference method* is obtained which is by definition an explicit multistep method. Central difference schemes are popular in explicit finite element software programs [30]

2.5.3 Newton-Raphson iteration

Recall the nonlinear equation of motion 2.9. The positions, velocities and accelerations are dependent of each other and the coefficient matrices are no longer constant. The dynamic equation can be rewritten to *residual form*

$$\boldsymbol{r}(\boldsymbol{u}) = \boldsymbol{M}\ddot{\boldsymbol{u}}(t) + \boldsymbol{f}(\boldsymbol{u}, \dot{\boldsymbol{u}}) - \boldsymbol{g}(\boldsymbol{u}, t) = 0$$

(2.24)
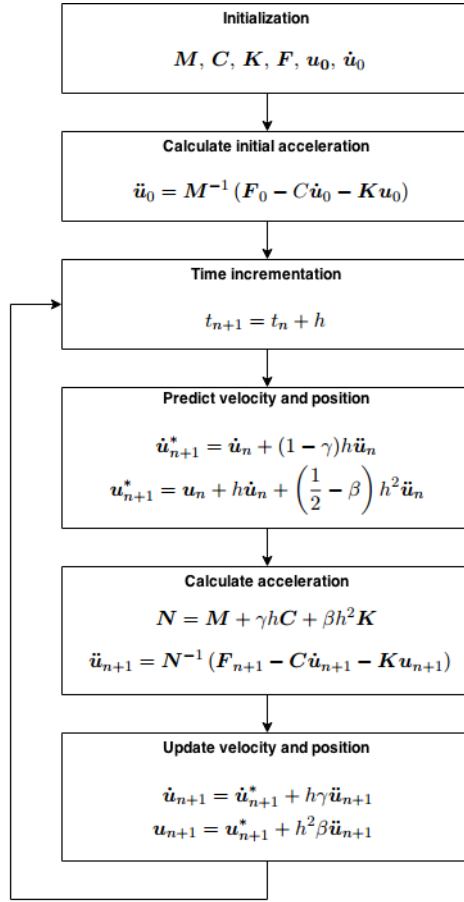
Figure 2.2: The Newmark integration scheme for linear structural dynamics

The Newmark implicit scheme can be extended to nonlinear problems by predicting values for the positions, velocities and accelerations and performing *Newton-Raphson iterations* on the residual equation 2.24.

$$u_{n+1}^k + \Delta u^k \qquad \dot{u}_{n+1}^k + \Delta \dot{u}^k \qquad \ddot{u}_{n+1}^k + \Delta \ddot{u}^k \tag{2.25}$$

At each iteration step k corrections are calculated for the positions, velocities and accelerations by the linearized system of equations

$$J \Delta u^k = -R\left(u_{n+1}^k\right) \tag{2.26}$$

where J is the Jacobi matrix given by

$$J = \frac{\partial r}{\partial u} = \frac{\partial f}{\partial u} + \frac{\partial f}{\partial \dot{u}} \frac{\partial \dot{u}}{\partial u} + M \frac{\partial \ddot{u}}{\partial u} - \frac{\partial g}{\partial u} \tag{2.27}$$

where

$$\boldsymbol{K}_t = \frac{\partial \boldsymbol{f}}{\partial \boldsymbol{u}} \quad and \quad \boldsymbol{C}_t = \frac{\partial \boldsymbol{f}}{\partial \dot{\boldsymbol{u}}} \tag{2.28}$$

is the tangent stiffness matrix and tangent damping matrix respectively. By introducing the Newmark integration relationships the Jacobi matrix can be shown to be [8]

$$\boldsymbol{J} = \boldsymbol{K}_t + \frac{\gamma}{\beta h} \boldsymbol{C}_t + \frac{1}{\beta h^2} \boldsymbol{M} \tag{2.29}$$

The corrections are thus calculated as

$$\Delta \boldsymbol{u}^k = \boldsymbol{J}^{-1} \left(-\boldsymbol{r}^k \right) \tag{2.30a}$$

$$\Delta \dot{\boldsymbol{u}}^k = \frac{\gamma}{\beta h} \Delta \boldsymbol{u}^k \tag{2.30b}$$

$$\Delta \ddot{\boldsymbol{u}}^k = \frac{1}{\beta h^2} \Delta \boldsymbol{u}^k \tag{2.30c}$$

Convergence criteria

Corrections are calculated for a time step until the convergence requirement is reached.

The implicit Newmark method with Newton-Raphson iterations are summarized schematically in figure 2.3

2.5.4   Discrete Fourier transform

The numerical time integration of the equations of motion produces time history of the motion of the system. This response will consist of combinations of vibration with different frequencies and may be difficult to read. Using *fourier transformation* a function in the time domain can be converted into the frequency domain and vice versa. The fourier transform and its inverse

is given by

$$F(\omega) = \frac{1}{2} \int\limits_{-\infty}^{\infty} f(t)e^{-i\omega t}dt \qquad (2.31a)$$

$$f(t) = \int\limits_{-\infty}^{\infty} F(\omega)e^{i\omega t}d\omega \qquad (2.31b)$$

More practically however, is the *Discrete fourier transform (DFT)* which takes a list of N discrete samples to calculate the Fourier transform, and is thus suitable for numerical analysis. The *Cooley-Tukey algorithm* demonstrated in 1965 [4] is a very efficient way of calculating the Fourier transform by the *fast Fourier transform (FFT)*. It was demonstrated that the DFT required N^2 operations while the FFT only required $NlogN$ operations [4] which can have a massive affect on the time required when used on large data sets. For details of the algorithms, refer to the citations.

It is important to note that according to the *Shannon Sampling Theorem*, upper frequency limit to the discrete fourier transform is half the sampling frequency, known as the *Nyquist frequency* [14].
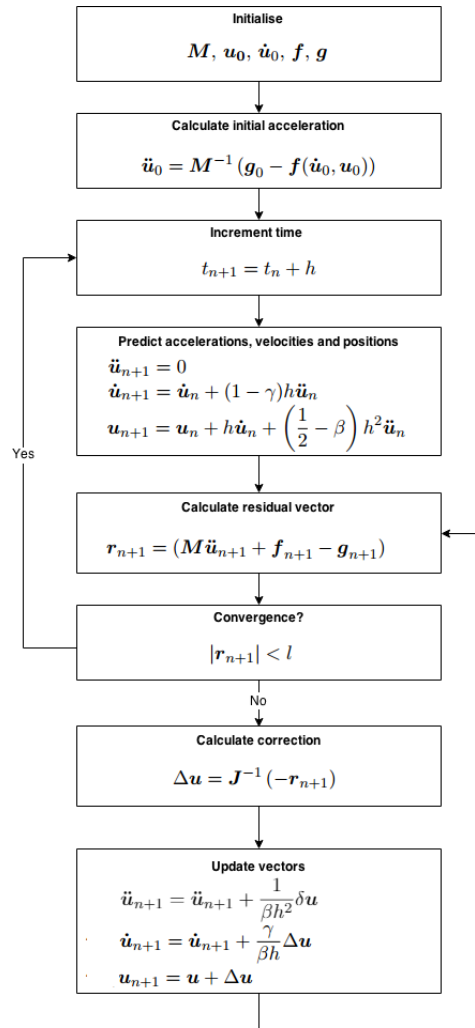
Figure 2.3: The Newmark integration scheme for nonlinear structural dynamics

Chapter 3

Camshaft modelling

3.1 Introduction

Modelling rotating structures and its behaviour has been studied for centuries and has developed into a separate field of applied mechanics known as *rotor dynamics*. One of the most important concerns in rotor dynamics is the assumptions and choices of DOFs for producing sufficiently accurate results. Of particular interest is the *critical speeds* at which resonance occur. The deformation of a shaft increases as the operating speed is approaching one of the critical speeds, and if the deflections are big enough, the shaft may be regarded as a *flexible rotor*. If the deformation is negligible however, the shaft is considered rigid. As the operating speed of a shaft is increased beyond the first critical speed, different sources of excitation is seen, e.g. self-excited vibrations from internal damping as studied by Newkirk [22] and oil-whip in the journal bearings. Asymmetry of mass from cams on the camshafts introduces parametrical excitations and can also cause unstable vibrations [36].

The medium-speed diesel engine camshaft is relatively slowly rotating and its dynamic behaviour is expected to be dominated by the external forces.

3.2 Material

Material selection for camshaft production is largely govern by the material's resistance against wear. The camshaft is modelled in steel with mechanical properties as described in table 3.1.

Modulus of elasticity [MPa]	210 000
Poisson's ratio [mm/mm]	0.3
Mass density [10^3 kg/m^3]	7.85

Table 3.1: Camshaft material

3.3   One dimensional model

The camshaft is modelled as a linear system of concentrated masses connected with idealised springs and dampers to represent the shaft flexibility and friction respectively. Transverse deflection of the shaft is neglected as the bearings and bearing houses are rigid. The first model is thus a pure torsional vibration analysis (TVA). The excitation torques on the camshaft are given as a function of the angular position of the shaft, and is thus a function of time through the nominal rotational speed of the system.

3.3.1   Kinetic and Potential Energy

The kinetic energy for a rotating element on the shaft is given by

$$T = \frac{1}{2}\left(I_i\dot{\theta}_i\right) \tag{3.1}$$

where θ_i is the angular velocity in the reference frame rotating at the nominal speed of the shaft Ω.

The potential energy is related to the twisting of the shaft sections interconnecting the mass stations and is given by

$$V = \frac{1}{2}K_i\left(\theta_i - \theta_{i-1}\right)^2 \tag{3.2}$$

3.3.2   Equations of motion

By differentiating the Lagrangian 2.5 one obtains the equations relating the motion for each mass station. Se figure 3.1

Figure 3.1: Schematic of the lumped mass model of the camshaft

$$
\begin{aligned}
I_g\ddot{\theta}_g + c_g\dot{\theta}_g - c_g\dot{\theta}_b + k_g\theta_g - k_g\theta_b &= 0 \\
I_b\ddot{\theta}_b - c_g\dot{\theta}_g + (c_g + c_b)\dot{\theta}_b - c_b\dot{\theta}_f - k_g\theta_g + (k_g + k_b)\theta_b - k_b\theta_f &= 0 \\
I_f\ddot{\theta}_f - c_b\dot{\theta}_b + (c_b + c_f)\dot{\theta}_f - c_f\dot{\theta}_e - k_b\theta_b + (k_b + k_f)\theta_f - k_f\theta_e &= 0 \\
I_e\ddot{\theta}_e - c_f\dot{\theta}_f + (c_f + c_e)\dot{\theta}_e - c_e\dot{\theta}_i - k_f\theta_f + (k_f + k_e)\theta_e - k_e\theta_i &= 0 \\
I_i\ddot{\theta}_i - c_e\dot{\theta}_e + (c_e + c_i)\dot{\theta}_i - c_i\dot{\theta}_{end} - k_e\theta_e + (k_e + k_i)\theta_i - k_i\theta_{end} &= 0 \\
I_{end}\ddot{\theta}_g - c_i\dot{\theta}_i + c_i\dot{\theta}_{end} - k_i\theta_i + k_i\theta_{end} &= 0
\end{aligned}
\tag{3.3}
$$

By lumping the masses, the mass matrix in equation 2.8 will be diagonal as apparent in the equations of motion for the camshaft (3.3)

$$
\boldsymbol{M} = diag(I_1, I_2, ..., I_n) \tag{3.4}
$$

where I is the inertia off-diagonal matrix elements are zero. The resulting stiffness matrix $\boldsymbol{K}$ is a tridiagonal (bandwidth of three) matrix on the somewhat shortened form

$$
\boldsymbol{K} = \begin{bmatrix}
k_1 & -k_1 & & & & \\
-k_1 & (k_1 + k_2) & -k_2 & & & \\
& -k_2 & (k_2 + k_3) & -k_3 & & \\
& & & \ddots & & \\
& & & & & -k_{n-1} \\
& & & & -k_{n-1} & k_{n-1}
\end{bmatrix}
\tag{3.5}
$$

The damping matrix is also a tridiagonal matrix

$$\boldsymbol{C} = \begin{bmatrix} c_1 & -c_1 & & & & \\ -c_1 & (c_1 + c_2) & -c_2 & & & \\ & -c_2 & (c_2 + c_3) & -c_3 & & \\ & & & \ddots & & \\ & & & & & -c_{n-1} \\ & & & & -c_{n-1} & c_{n-1} \end{bmatrix} \tag{3.6}$$

The damping matrix is on the same form as the stiffness matrix, with the addition of external friction in the journal bearings (see figure 3.1.

Since production drawings for the camshaft are given, the mass coefficients and stiffness coefficients are found numerically using the finite element program *Abaqus 6.14*. The masses of the shaft sections connecting the idealised mass stations along the camshafts are split by assuming that the idealised mass stations connected at each end takes half the mass each.

3.4   Damping

Finding values for the mass and stiffness matrices are trivial, however this is not the case for the damping coefficients. The camshaft model inhibits both internal (material) damping and viscous friction. The internal damping is due to energy dissipation in the twisting of the flexible shafts and viscous damping is energy loss in the journal bearings. Damping is often kept out of the Lagrange equation (equation 2.4) and then introduced to the system of equations through modal damping ratios.

The damping is assumed to be proportional (*Rayleigh damping*) to the mass and stiffness matrices.

$$\boldsymbol{C} = a\boldsymbol{M} + b\boldsymbol{K} \tag{3.7}$$

where the coefficients a and b *Rayleigh coefficients*. Proportional damping has been shown to be an adequate approximation in many cases [7]. In the case of $b = 0$, $a \neq 0$ the damping is proportional to the masses and the represents a system where the masses are connected to ground through viscous dampers (see $c_f ric$ in figure 3.1. In the case where $a = 0$ and $b \neq 0$ represents a system where the damping coefficients are proportional to the stiffness and may be modelled as discrete dampers in parallel with the spring elements. The Rayleigh damping coefficients a and b must nonetheless be chosen based on qualified guesses or physical experiments on the system.

When assuming proportional damping, the damped eigenvectors are the same as the undamped eigenvectors, and by orthogonal transformation of the resulting equation, uncoupling 2.8 the damping ratio can be written on the form

$$\xi_i = \frac{a}{2\omega_i} + \frac{b\omega_i}{2} \qquad (3.8)$$

where ξ_i is the damping ratio of the ith natural frequency, ω_i. It is clear from equation 3.8 that for higher natural frequencies ω_i, the first term on the right hand side of equation 3.8 becomes increasingly dominant, but for lower frequencies the left term is dominant. I.e. a affects the lower vibration modes and b affects the higher ones. Figure 3.2 shows that a plot of equation 3.8 for $a = 0.05$ and $b = 0.05$. For low frequencies the damping variation is nonlinear but approaches the linear asymptote as the frequencies increases.
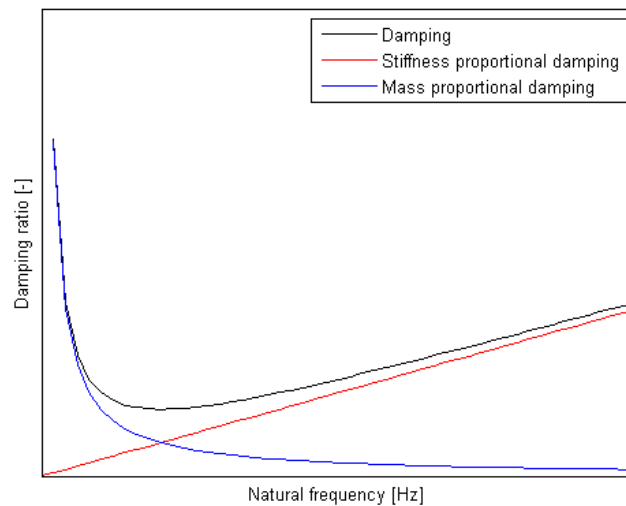

Figure 3.2: Variation of damping ratio with natural frequency for a typical system

By knowing (by measure for instance) two damping ratios ξ_1 and ξ_2 corresponding to the natural frequencies ω_1 and ω_2, the Rayleigh damping

coefficients a and b. By inserting into equation 3.8 one obtains

$$\begin{aligned}
a &= \frac{2\omega_1\omega_2}{\omega_2^2 - \omega_1^2} \left(\omega_2\xi_1 - \omega_1\xi_2\right) \\
b &= \frac{2}{\omega_2^2 - \omega_1^2} \left(\omega_2\xi_2 - \omega_1\xi_1\right)
\end{aligned} \tag{3.9}$$

For structures with many degrees of freedom it is unnecessary to account for all modes. The first modes are generally dominant with its mass participation and higher modes can be neglected. The number of significant modes, however, varies depending on the problem, but may be estimated by iteration on a first guess on the number of modes [2].

By assuming purely mass based or stiffness based damping, damping coefficients can be calculated by e.g. taking damping to be 1% of critical damping for the fundamental frequency. Results based on the frequencies in section 5.1 are shown in the table below for $\xi = 0.01$ of the first eigenfrequency.

Cylinders	a	b
6	21.16	1.89e-5
7	18.74	2.13e-5
8	16.88	2.37e-5
9	15.38	2.60e-5
10	14.16	2.83e-5

Table 3.2: Rayleigh damping coefficients assuming $\xi_1 = 0.01$

In the following table, the Rayleigh coefficients are calculated by assuming the damping to be proportional to both the mass and stiffness of the system. Damping ratio is taken to be 1% of critical damping for the first natural frequency and 2% for the second.

Cylinders	First freq.y [rad/s]	Second Freq. [rad/s]	a [-]	b [-]
6	1046.6	2579.7	29.69	2.35e-6
7	925.5	2242.8	24.48	2.72e-6
8	859.9	2068.0	22.00	2.95e-6
9	757.6	1784.8	17.54	3.43e-6
10	719.0	1672.0	15.60	3.67e-6

Table 3.3: Rayleigh damping coefficients assuming $\xi_1 = 0.01$ and $\xi_2 = 0.02$

3.5   Excitation forces

Each cam on the shaft is subjected to a variational load as the shaft rotates. In a PLN system the injection pump represents the largest loads, compared to the exhaust and air inlet valves. The crankshaft excites the system with harmonics related to the engine rotational speed, these are however neglected and only the excitations from the valves and injection pump are considered.
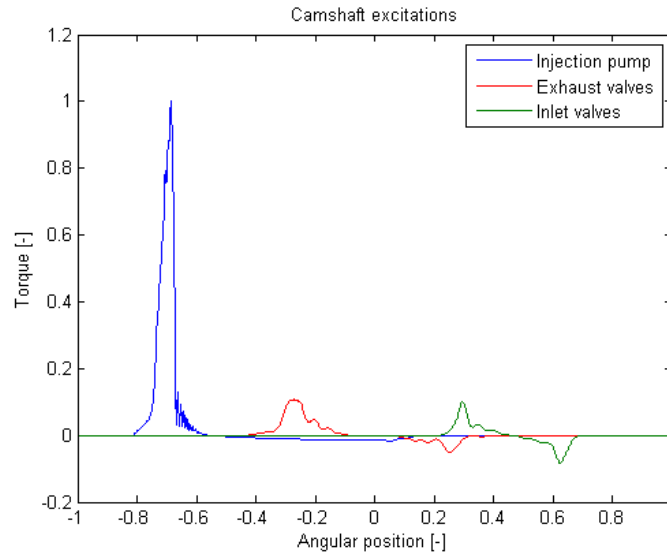
Figure 3.3: Torques on the camshaft section unit

Figure 3.3 shows the normalised torque acting on the exhaust, inlet and injection pump cam on each cylinder section as a function of angular position. It is clear that the injection pump is the most significant excitation on the camshaft system. Depending on camshaft rotational speed, the cams will excite the camshaft with harmonics related to the firing engine frequency. The torques in figure 3.3 are related to camshaft rotating at 375 rpm. There are sources of oscillatory behaviour observed in the torque plot, owing to the valvetrain dynamics. Valvetrain flexibility causes wind-down as is especially apparent as the injection pump roller lift returns to zero [16]. The camshaft is thus excited with several frequencies during operation.

The response of the camshaft is depending on the frequencies of excitation. This is illustrated with the frequency response function of a simple harmonic oscillator, see figure 3.4, derived from equation 2.8. The graph illustrates the structural steady state response X to the applied force F as a function of frequency ratio $\Omega = \frac{\omega}{\omega_n}$ for different values of damping ξ.

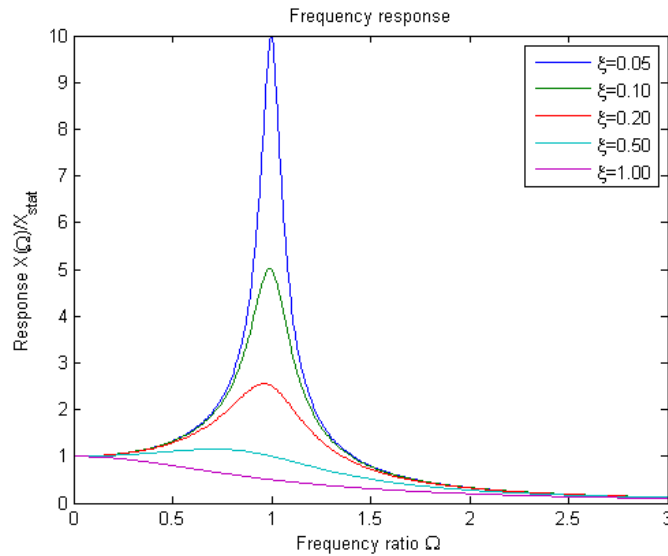Figure 3.4: Frequency response function of simple harmonic oscillator

It is clear from figure 3.4 that the response of a structure is depending on frequency and damping. When the frequency of excitation is very low, the response approaches the static response, thus the response is governed by the stiffness. If the frequency of excitation is close to the natural frequency however, the response increases and is heavily influenced by the damping ratio xi. For very high frequencies compared with the natural frequency, the response is governed by inertia as the structure will not have time to react to the high frequency excitations.

The *firing order* of the cylinders is also expected to has an effect on the camshaft dynamics. Firing order is in engine design often chosen to minimise the vibration and to balance the engine for smooth running. The firing order is an important consideration in the crankshaft design, but also affects the camshaft.

3.6 Finite element assessment

The camshaft was modelled in *SolidWorks* and imported into Abaqus in order to numerically find mass and stiffness values for the discrete model, see figure 3.5. The three dimensional model was produced in accordance with production drawings supplied from Bergen Engines. Each part in the camshaft assembly is represented by a deformable body with a reference point

in each end along its axis of rotation. These reference points are connected to the mounting surfaces through kinematic coupling constraints and to the reference points of the adjacent part using rigid connectors.
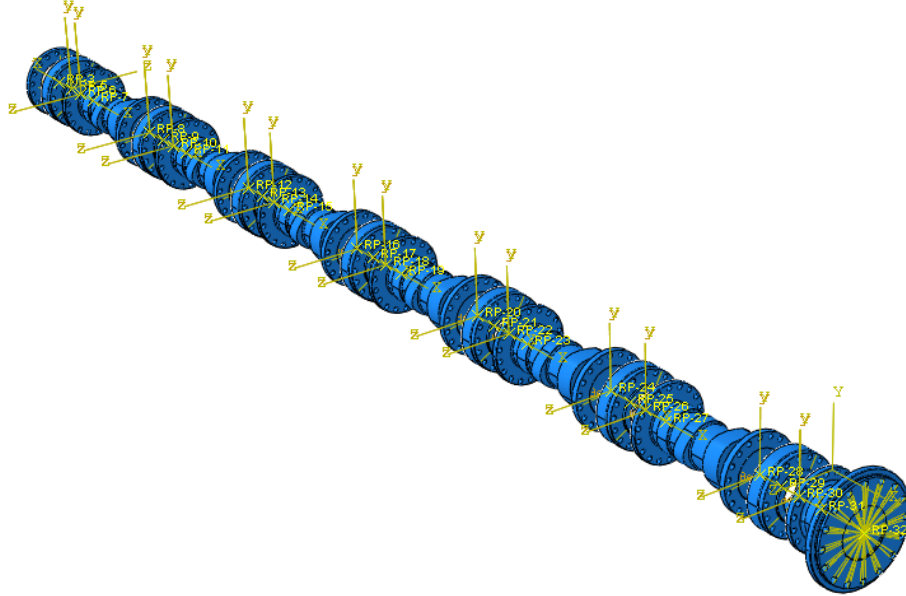
Figure 3.5: 6 cylinder camshaft modelled in Abaqus

The parts were freely meshed with quadratic tetrahedral elements with approximate global size of 16 mm, see section 2.4.

To obtain the stiffness for each discrete spring interconnecting the lumped masses, the corresponding shaft section is extracted from the model described. The twisting stiffness is calculated by taking each shaft section from the center of a mass center to the middle of the next. A static angular deflection of $1rad$ is then applied and the resulting reaction moment is registered. Thus, stiffness is calculated as

$$k = \frac{\theta}{T} \qquad (3.10)$$

where θ is the angular deflection and T is the resulting torque.

3.7   Adding complexity

The single degree of freedom model of the camshaft assumes that the lateral deflections of the camshafts are neglegible. There will, however, also be transverse motion in the camshaft and in the ideal model, solutions for the torsional vibration and bending vibration are solved simultaneously (combined TVC and LVC). This could include detailed inclusions of e.g. contact conditions between the cam profiles and the follower and lubrication conditions in bearings. Lubricated contact conditions are especially complicated and solved with *Reynolds equation*. While mathematically interesting, these complex addons to a multi-cylinder system would considerably increase the computational time, sometimes to the impractical extent [31].

Chapter 4

Gear transmission model

4.1 Introduction

Harris [9] considered three sources of internal sources of vibration in meshing spur gears; Periodic velocity ratio due to manufacturing errors, periodic variation in mesh stiffness and non-linearities in mesh stiffness, like loss of contact.

Harris was one of the first to predict excitations in gears due to stiffness variation in the teeth. He performed tests and observed the vibrations due to errors in velocity ratio, but the modes corresponding to the varying meshing stiffness and non-linearities in tooth stiffness were not found in the experiments due to high damping.

Harris suggested that vibration occurred in ideal spur gears without external excitations if the damping was less than 0.07 of critical damping ratio.

In 1967 Opitz [24] presented a single degree of freedom model with viscous damping, time varying mesh stiffness, *backlash* and gear error included. He solved the non-linear equations on an analog computer and confirmed the results with measurements and other analytical models at the time.

Munro [21] showed experimentally that tooth separation in spur gears with backlash occurred when the mean load was less than the design load, which was previously stated by Harris [9].

Wang and Cheng [35] used in 1981 a torsional vibratory model being lumped and of single degree but used the finite element methods to obtain the varying tooth stiffness. Although the aim was to develop computer code and to study

lubrication film thickness, surface temperature etc., they determined the effects of load sharing of the teeth, variable mesh stiffness and tooth profile errors on the variations of dynamic tooth load.

Umezawa et al. [32] included periodic variation of mesh stiffness and a constant damping in the single degree of freedom model for torsional vibrations. They used a newly developed measuring device to obtain the gear error and accurately predicted the dynamic behaviour of a spur gear pair using the *Runge-Kutta-Gill* numerical integration method.

Ösgüven and Houser [37] published in 1987 a paper describing the mathematical models used in gear dynamics. A large number of publications was reviewed and a description of the models was given, including a general classification in addition to the different objectives and parameters involved.

Ösgüven and Houser summarized the different models into the following categories.

(1) *Simple Dynamic Factor models* in which the objective is to find a dynamic factor to determine the root stresses in the gear teeth. These studies relied largely on empirical and semi-empirical data. These methods are mostly covered by the industry standards [12, 5]

(2) *Models with Tooth Compliance* which usually modelled the gears with one degree of freedom, having the tooth stiffness as the only potential energy storing element. The compliance of shafts, bearings etc. was thus neglected.

(3) *Models for Gear Dynamics* included the flexibilities of other elements in addition to the tooth compliance, most commonly the torsional flexibility of shafts.

(4) *Models for Geared Rotor Dynamics*. In rotor dynamic models with more than one degree of freedom transverse vibration of shafts and whirling are considered.

(5) *Models for Torsional Vibrations*. In these models, the flexibility of the gears was neglected and thus reduced the system to a torsional vibration problem with rigid gears.

The authors emphasizes that a clear classification of the different models reviewed was difficult and many mathematical models were a combination of the categories mentioned. Some studies aims at finding the system natural frequencies and therefore only considered free vibration. In most studies, however, the time response of the system is of interest. Excitation forces due to gear errors and tooth stiffness variation during meshing cycle is determined.

Some studies also included nonlinear effects like loss of tooth contact.

Ösgüven and Houser also stated that even the simpler models in category (2) showed good agreement with physical experiments. However, it was emphasized that adding degrees of freedom for shaft and bearing flexibilities were necessary for more general models, unless the stiffness of these elements was very high or very low compared with the other sources of compliance.

In some analyses in the literature, Ösgüven and Houser reported the models to have rigid disks representing the inertia of gears and shafts and torsional springs representing the torsional flexibilities of the shaft. These models were used as *normal mode analyses* to find the systems natural frequencies and the corresponding mode shapes.

Several authors have published papers on the analysis of torsional stiffness in a pair of involute spur gear mesh using the finite element method, i.e. Howard and Wang [34]. They presented a discussion on different methods for modelling the torsional stiffness in the meshing gears. They showed that the gear body stiffness and the relative strain between the teeth in mesh should be included in the model for an accurate stiffness prediction. Torsional mesh stiffness and the *tooth handover region* was found to be depending on the load.

The mesh stiffness relies on a number of factors, including the applied load, material properties, gear face width, profile modifications, number of teeth in contact etc., which give rise to a complicated function describing the mesh stiffness. In practice however, two values for stiffness is often regarded as sufficient [15], describing the stiffness when either one or two teeth pairs are in contact. This variation is often small compared to the average stiffness and is thus neglected in many cases [15].

4.2   Two Degrees of freedom-model

Simple mathematical models of the gear drive in which shaft and bearing flexibilities were neglected showed good agreement with experimental measurements [37] and is therefore considered the next appropriate step to add to the camshaft model.

The camshaft gear drive in most medium-speed diesel engines consists of four gear wheels. The crankshaft gear wheel transmits power to a big idler gear which is coaxially connected with a smaller idler gear that transmits power to the camshaft gear wheel. See table 4.1. Thus, there are two separate gear meshes which interacts and excites the system. Each gear ($i = 1 - 4$) with

	Pinion	**Gear**	**Pinion**	**Gear**
	Crankshaft	Big idler	Small idler	Camshaft
Module m	8	8	9	9
Number of teeth z	59	64	34	59
Pressure angle α	20	20	20	20
Profile shift coeff. x	-0.626	-0.626	-0.082	-0.082
Min. backlash BL_{min} [mm]	0.15	0.15	0.15	0.15
Max. backlash BL_{max}[mm]	0.43	0.43	0.43	0.43
Face width [mm]	90	88	135	130
Base diameter d_b [mm]	443.535	511.193	287.546	498.977
Rotational freq. Ω [Hz]	12.50	10.86	10.86	6.25

Table 4.1: Camshaft gear drive data

it's moment of inertia I_i are allowed to vibrate in torsional mode. Bearings and shafts are thus assumed to be rigid. See figure 4.1.
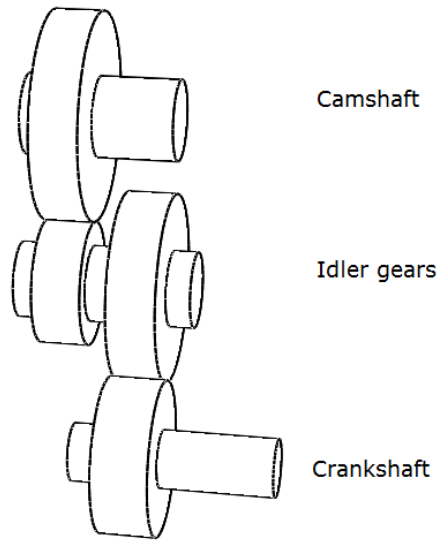

Figure 4.1: Gear drive assembly

In earlier literature, it was common practice to define the degrees of freedom in gear dynamics as the elastic motion along the pressure line of the meshing gears and thereby avoiding the rigid body mode (see equation 4.2). For consistency in the matrix system with the camshaft, one rotational degree of freedom is added for each of the gears in the gear drive. The distance between the idler gears on the idler shaft is short and the shaft is stiff. The

angular rotation of the two idler gears are thus assumed to be equal:

$$\theta_2 = \theta_3 \tag{4.1a}$$

$$I_{23} = I_1 + I_2 \tag{4.1b}$$

$$\tag{4.1c}$$

One degree of freedom is introduced for each mesh, and the relative displacement δ_i between two gears in mesh along its line of action may be written as

$$\delta_1 = r_2\theta_2 - r_1\theta_1 \tag{4.2a}$$

$$\delta_2 = r_3\theta_3 - r_2\theta_2 \tag{4.2b}$$

Where r_i and θ_i are the base radii and angular rotation of gear i ($i = 1, 2, 3, 4$).

4.2.1 Backlash

Due to gear backlash there is a possibility for tooth separation (contact loss) and backside tooth contact during operation. Backside contact in high load gears are rare [19], but due to the time varying torques on the camshaft from injection pumps and valve springs, backside contact and hammering are expected.

The non-linear effect of loss of contact may be expressed as a piecewise linear function with a dead zone. Mathematically, the backlash functions may be expressed as

$$g_1\left[\delta_1(t)\right] = \begin{cases} \delta_1(t) - b_{n1} & \text{if } \delta_1(t) > b_{n1} \\ 0 & \text{if } -b_{n1} \leq \delta_1(t) \geq b_{n1} \\ \delta_1(t) + b_{n1} & \text{if } \delta_1(t) < b_{n1} \end{cases} \tag{4.3a}$$

$$g_2\left[\delta_2(t)\right] = \begin{cases} \delta_2(t) - b_{n2} & \text{if } \delta_2(t) > b_{n2} \\ 0 & \text{if } -b_{n2} \leq \delta_2(t) \geq b_{n2} \\ \delta_2(t) + b_{n2} & \text{if } \delta_2(t) < b_{n2} \end{cases} \tag{4.3b}$$

where $2b_{n1}$ and $2b_{n2}$ are the widths of the dead zone (backlash) of mesh 1 and 2 respectively.

$k_1(t)$ and $k_2(t)$ are the time varying stiffnesses and c_1 and c_2 is the constant damping of each gear mesh acting along the line of action.

The equations of motion for this system can be expressed as

$$I_1\ddot{\theta}_1(t) + r_1 c_1 \left[r_1\dot{\theta}_1(t) - r_2\dot{\theta}_2(t) \right] + r_1 k_1(t) g_1 \left[\delta_1(t) \right] = T_1(t) \qquad (4.4a)$$

$$I_{23}\ddot{\theta}_2(t) + r_2 c_1 \left[r_1\dot{\theta}_1(t) - r_2\dot{\theta}_2(t) \right] + r_2 k_1(t) g_1 \left[\delta_1(t) \right] +$$
$$r_3 c_2 \left[r_3\dot{\theta}_2(t) - r_4\dot{\theta}_4(t) \right] + r_3 k_2(t) g_2 \left[\delta_2(t) \right] = T_{23}(t) \qquad (4.4b)$$

$$I_4\ddot{\theta}_4(t) + r_4 c_2 \left[r_3\dot{\theta}_2(t) - r_4\dot{\theta}_4(t) \right] + r_4 k_2(t) g_2 \left[\delta_2(t) \right] = T_4(t) \qquad (4.4c)$$

Where $k_1(t)$ and $k_2(t)$ are the time varying stiffnesses for the first and second gear meshes respectively. The damping is assumed to be time-invariant.
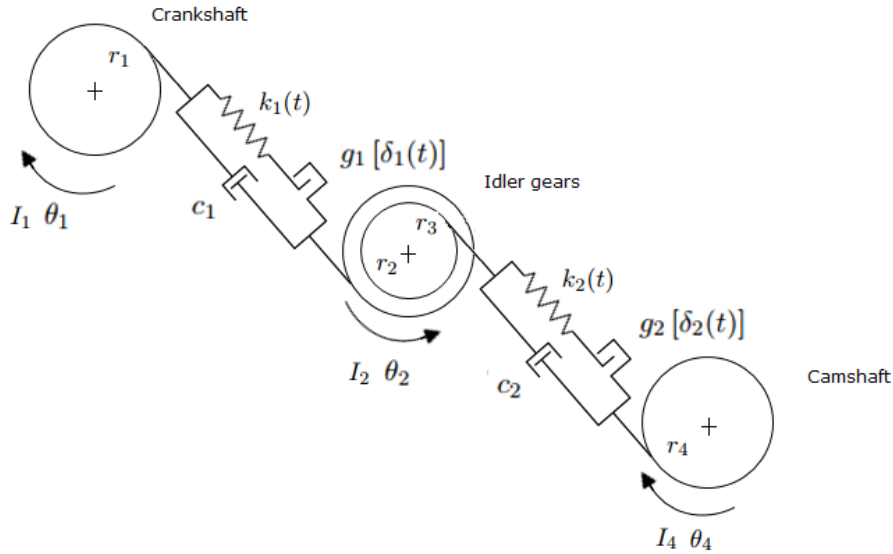

Figure 4.2: Gear drive model with two degrees of freedom

By inserting the equations for the backlash functions $g_1 \left[\delta_1(t) \right]$ and $g_2 \left[\delta_2(t) \right]$ (equation 4.3), the nonlinear nature of the backlash introduces contributions

to the tangent stiffness and internal forces

$$I_1\ddot{\theta}_1 = -c_1 r_1 (r_1 \dot{\theta}_1 - r_2 \dot{\theta}_2) + h_1 r_1 + T_1$$
$$I_1\ddot{\theta}_1 + c_1 r_1^2 \dot{\theta}_1 - c_1 r_1 r_2 \dot{\theta}_2 + h_1 r_1 = T_1 \tag{4.5a}$$

$$I_2\ddot{\theta}_1 = -c_1 r_2 (r_2 \dot{\theta}_2 - r_1 \dot{\theta}_1) - h_1 r_2 + h_2 r_3 + c_2 r_3 (r_4 \dot{\theta}_4 - r_3 \dot{\theta}_3) + T_2$$
$$I_2\ddot{\theta}_1 + c_1 r_2^2 \dot{\theta}_2 - c_1 r_1 r_2 \dot{\theta}_1 - c_2 r_3 r_4 \dot{\theta}_4 + c_2 r_3^2 \dot{\theta}_3 + h_2 r_3 + h_1 r_2 + T_2 \tag{4.5b}$$

$$I_4\ddot{\theta}_4 = -c_2 r_4 (r_4 \dot{\theta}_4 - r_3 \dot{\theta}_3) - h_2 r_4 + T_4$$
$$I_4\ddot{\theta}_4 + c_2 r_4^2 \dot{\theta}_1 - c_2 r_4 r_3 \dot{\theta}_3 - h_2 r_4 = T_4 \tag{4.5c}$$

The equations are further expanded by rewriting the nonlinear terms h_1 and h_2 and by introducing coefficients to govern the contact conditions in the gear mesh:

$$h_1 = k_1(t)g_1\left[\delta_1(t)\right] = k_1(t)b_1\beta_1 + k_1(t)r_2\theta_2\kappa_1 - k_1(t)r_1\theta_1\kappa_1 \tag{4.6a}$$
$$h_2 = k_2(t)g_2\left[\delta_2(t)\right] = k_2(t)b_2\beta_2 + k_2(t)r_4\theta_4\kappa_2 - k_2(t)r_3\theta_3\kappa_2 \tag{4.6b}$$

where β_1 and β_2 are the "contact condition coefficients" for the two gear meshes governing internal forces. κ_1 and κ_2 is the contact condition coefficients affecting the tangent stiffness matrix. Thus, the nonlinear force vector $\boldsymbol{h}$ in the equilibrium equation may be expanded.

$$\boldsymbol{K_t} = \begin{bmatrix} k_1(t)r_1^2\kappa_1 & -k_1(t)r_1 r_2\kappa_1 & 0 \\ -k_1(t)r_1 r_2 k_1\kappa_1 & k_1(t)r_2^2\kappa_1 + k_2(t)r_3^2\kappa_2 & -k_2(t)r_3 r_4\kappa_2 \\ 0 & -k_2(t)r_4 r_3\kappa_2 & k_2(t)r_4^2\kappa_2 \end{bmatrix} \tag{4.7}$$

and the *internal force vector* is given by

$$\boldsymbol{F_{int}} = \left\{ \begin{array}{c} -k_1(t)b_1 r_1\beta_1 \\ k_1(t)b_1 r_1\beta_1 - k_2(t)b_2 r_3\beta_2 \\ k_2(t)b_2 r_4\beta_2 \end{array} \right\} \tag{4.8}$$

where the coefficients κ and β are derived from the contact conditions in the piecewise linear functions 4.3 and given by:

$$\kappa_1\left[\delta_1(t)\right] = \begin{cases} 1 & \text{if } |\delta_1| > b_{n1} \\ 0 & \text{if } |b_{n1}| \leq b_{n1} \end{cases} \tag{4.9a}$$

$$\kappa_2\left[\delta_2(t)\right] = \begin{cases} 1 & \text{if } |\delta_1| > b_{n1} \\ 0 & \text{if } |b_{n1}| \leq b_{n1} \end{cases} \tag{4.9b}$$

$$\beta_1\left[\delta_1(t)\right] = \begin{cases} -1 & \text{if } \delta_1 > b_{n1} \\ 0 & \text{if } -b_{n1} \leq \delta_1 \geq b_{n1} \\ 1 & \text{if } \delta_1 < b_{n1} \end{cases} \tag{4.10a}$$

$$\beta_2\left[\delta_2(t)\right] = \begin{cases} -1 & \text{if } \delta_2 > b_{n2} \\ 0 & \text{if } -b_{n2} \leq \delta_2 \geq b_{n2} \\ 1 & \text{if } \delta_2 < b_{n2} \end{cases} \tag{4.10b}$$

By inserting into the linear equation of equilibrium 2.8, the system becomes nonlinear due to contact conditions and time-varying stiffness. It is clear that the resulting system of equations are reduced to the standard linear case when the backlash b is set to 0 and the stiffness is assumed constant ($k(t) = k$). These equations are suitable for the numerical time stepping process as described in section 2.5.2, finding equilibrium at each point in time.

4.3   Mesh cycle stiffness

The teeth are assumed to be individually error free, i.e. the transmission error excites at meshing frequency and its higher harmonics only. As the gears rotate, parametric excitation is introduced due to time-varying compliance between the gear. This is mainly due to the number of teeth in contact during gear meshing not being constant, but is also varying as the contact point between two gear teeth moves along the tooth face. As the contact ratio of the gears increase, this stiffness variation becomes smaller. Hence, gear parameters such as the number of teeth, center distance, profile shift etc. can be modified to reduce parametric excitation due to varying stiffness.

This stiffness variation is often described by a periodic square function as shown in figure 4.5. This square function may furthermore be approximated by a sum of sines and cosines, a *Fourier series*. The stiffness may also be found using finite element software, which however can be quite time

consuming. The gears needs to have very fine mesh especially in the zone of contact between the teeth.

A number of methods for estimating the gear meshing stiffness is proposed in earlier literature, i.e. using cantilever beam theory [18]. With recent hardware developments and the availability of finite element procedures however, more accurate results may be produced. Finding the stiffness is still a complex matter numerically. Howard and Wang [34] used adaptive meshing where the elements near the contact areas between the two mating gears having elements as small as 0.0033 mm to deal with the chaotic non-linear effects in the contact area.

4.3.1 FEM modelling of gears

Values for the meshing stiffness of the two gear pairs have been found using finite element software. A semi-automatic method of modelling geometry in Abaqus is chosen. Having correct geometry is important, especially at contact surfaces between two mating gears and tooth fillet. A python script is made in order to facilitate sketching of the geometry (see appendix A.1). This script file is run in Abaqus, which loops through a text file with geometry defined as two dimensional coordinates. Spline is automatically drawn between the points resulting in a smooth line through the points. Tip relief is then added manually.

The gears are modelled as two-dimensional elements with plane strain. Global element size is 15 mm, but heavily refined in the tooth area (0.5 mm). Element size at the contact areas are 0.005 mm, see figure 4.3.
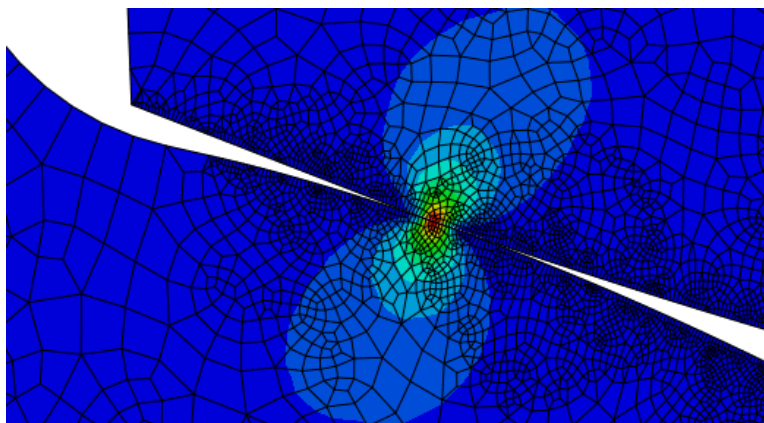

Figure 4.3: Small elements in the areas with Hertzian contact

The zones of single and double tooth contact for the mating gears are found by carefully rotating the pinion while having a small load to the gear. The point at which the gears switches from having two tooth pairs in contact to one pair is called the hand-over region and is observed during this rotational procedure. The positions of the gears are noted for the case of single tooth contact at the highest point of single tooth contact (HPSTC) and at double tooth contact, see figure 4.4.
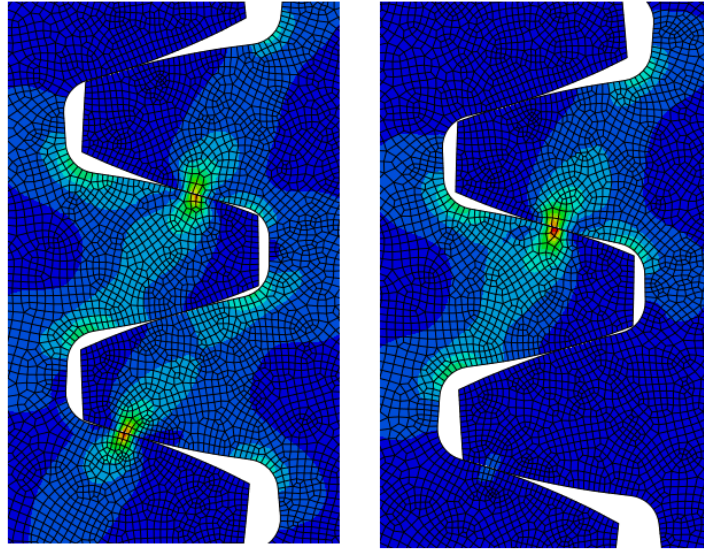

Figure 4.4: Single and double tooth contact in the first gear stage

A single analysis is then run for each case of contact in the gear meshes. In this analysis the pinion gear is restrained from motion while a torque of $1000Nm$ is applied to the gear. The mesh density is highly refined in the contact area to deal with the *Hertzian contact stresses*, see figure 4.3. The combined stiffness of the pinion and the gear can then be calculated as

$$K_{torsion} = \frac{M}{\Delta \omega} \quad (4.11)$$

where M is the reaction moment in the restrained pinion and $\Delta \omega$ is the angular position of the gear center node. To assess the mesh stiffness as a linear stiffness along the line of contact, the tangential force and linear

deformation is used.

$$k_{mesh} = \frac{F}{\delta} \tag{4.12}$$

where F is the forces acting on the teeth along the line of action and δ is the tooth deformation.

The results are given in the table below.

	Error	Moment	Torsional stiffness	Tooth deflection	Mesh stiffness
	[rad]	[Nm]	[Nm/rad]	[m]	[N/m]
Mesh 1					
Single	2.326e-5	8.677e2	3.731e7	5.944e-6	6.185e8
Double	1.389e-5	8.676e2	6.246e7	3.550e-6	1.035e9
Mesh 2					
Single	2.087e-5	5.763e2	2.761e7	5.207e-6	7.234e8
Double	1.876e-5	5.760e2	3.070e7	4.681e-6	8.042e8

Table 4.2: Measurements of stiffness on gear pairs

By using cantilever beam theory, the meshing stiffness may be approximated by two beams in series as

$$k_m = \frac{1}{\frac{1}{k_t} + \frac{1}{k_t}} \tag{4.13}$$

where the stiffness k_t is given by inserting gear parameters into the cantilever equation and thus obtaining

$$k_t = \frac{Ed^3p^3}{32(a+b)^4 \cos \alpha} \tag{4.14}$$

where d is the tooth width, a is the addendum height, b is the dedendum height and α is the pressure angle. As a comparison to the numerics in table 4.2, equation 4.13 and eqs. (4.13) and (4.14) gives $k_1 = 3.719e8$ and $k_2 = 14.755e8$ for gear mesh one and two respectively.

The two gear pairs in table 4.1 have high enough contact ratio for three teeth to come into contact at some points which further complicates the load sharing and hence the stiffness. For simplicity, the two gear pairs are assumed to alternate between having single and double tooth contact.

The base radii of the gears are thus assumed to be fixed with tooth stiffness as the gear compliance. This stiffness fluctuates with the gear mesh frequency $f_m = Z\Omega/60 = 2\pi\omega$ and can be expressed as a Fourier series approximation.

$$k_1(t) = k_{m1} + \sum_{n=1}^{N} \frac{k_{d1}}{n}(\cos n\omega t) + \sin(n\omega t) \tag{4.15a}$$

$$k_2(t) = k_{m2} + \sum_{n=1}^{N} \frac{k_{d2}}{n}(\cos n\omega t + \psi) + \sin(n\omega t + \psi) \tag{4.15b}$$

where k_{m1} and k_{m2} are the average stiffnesses and k_{d1} and k_{d2} are the variational stiffness. The square wave approximation to the time varying stiffness using the Fourier expansion with the first 10 harmonics and arbitrary meshing frequency is shown in the following figure. The phase between the two meshes are zero. Note that the resulting contact ratio is 1.5 but this can be modified.
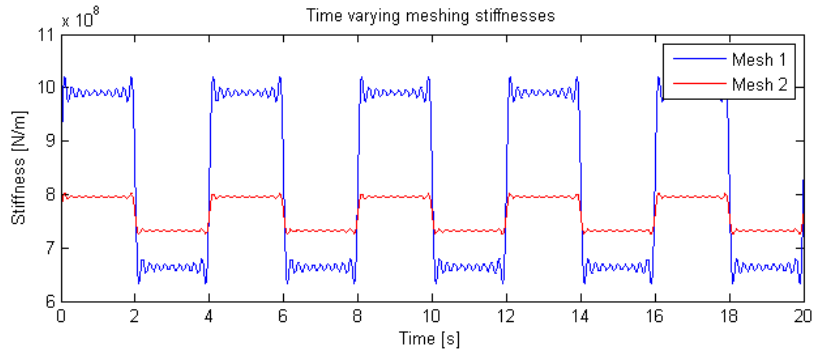

Figure 4.5: Fourier approximation of time-varying stiffness for the two gear pairs using 10 harmonics and zero phase

4.4 Numerical time integration

Given the non-linear nature of the equations of motion for the gear drive, direct numerical integration is preferred. Furthermore, since the gear meshing introduces nonlinearity to the overall system, an equilibrium iteration procedure needs to be included in the time stepping process, see figure 2.3.

In the time integration process a routine is introduced to check the contact conditions in each gear mesh according to equation 4.3. This function

takes three arguments; the position of the two gears and the backlash value associated with the gear pair. The function returns two coefficients, the stiffness matrix contribution coefficient and the force vector contribution coefficient. The returned stiffness coefficient matrix controls the tangent stiffness matrix depending on whether there is contact or not. If the conditions for contact loss are met, the stiffness vanishes. The nonlinearity of tooth separation also produces a vector of internal forces $\boldsymbol{N}$ which is added to residual force vector and used in the iteration process, see equation 2.30.

The expression for time varying stiffness from equation 4.15 is continuous, but overshoots for large steps (see figure 4.5. In discrete time stepping the simple stepping function (discontinuous) for the stiffness may be obtained by using

$$
\begin{aligned}
k_1(t) &= k_{m1} + k_{d1} * sign(\sin \omega_1 t) \\
k_2(t) &= k_{m2} + k_{d2} * sign(\sin \omega_1 t + \psi)
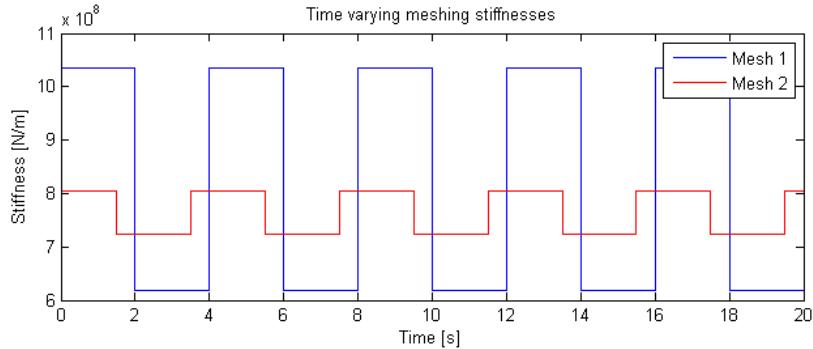\end{aligned}
\tag{4.16}
$$

Figure 4.6: Discontinuous stepping function for describing the time-varying stiffness

Portions of the Matlab code can be found in appendix, A.2.

4.4.1 Validation backlash model

The numerical methods for solving the nonlinear system introduced with the gears are benchmarked against *Fedem*. Fedem is a software package designed for modelling and simulation of finite element assemblies and multibody systems. A predictable model of the gears is made based on the classical

example of two lumped masses connected in series and to ground through discrete springs and dampers, see figure 4.7. Backlash is introduced to the system by a discontinuity in the springs and a time varying force is added to the second mass.
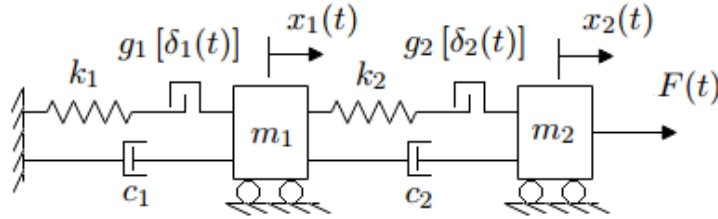

Figure 4.7: Simple two degree of freedom system with backlash

This simplified problem has two degrees of freedom, but an extra equation is introduced as a boundary condition to remove rigid body mode. Following the same conventions as introduced in section 4.2.1, the system matrices are given as

$$\boldsymbol{M} = diag(0, m_1, m_2) \tag{4.17a}$$

$$\boldsymbol{K} = \begin{bmatrix} 1 & 0 & 0 \\ 0 & k_1(t)\kappa_1 + k_2(t)\kappa_2 & -k_2(t)\kappa_2 \\ 0 & -k_2(t)\kappa_2 & k_2(t)\kappa_2 \end{bmatrix} \tag{4.17b}$$

$$\boldsymbol{C} = \begin{bmatrix} 0 & 0 & 0 \\ 0 & c_1 + c_2 & -c_2 \\ 0 & -c_2 & c_2 \end{bmatrix} \tag{4.17c}$$

$$\boldsymbol{F}_{int} = \left\{ \begin{matrix} 0 \\ k_1(t)b_1\kappa_1 - k_2(t)b_2\kappa_2 \\ k_2(t)b_2\kappa_2 \end{matrix} \right\} \tag{4.17d}$$

$$\boldsymbol{F}_{ext} = \{0 \quad 0 \quad F(t)\}^T \tag{4.17e}$$

$$\boldsymbol{F} = \boldsymbol{F}_{ext} - \boldsymbol{F}_{int} \tag{4.17f}$$

A force ramp is applied to the second mass from start to 1 second, held for 1 second and then released which sets the system into oscillatory motion.

Fedem model setup

In Fedem 7.11 the discrete masses are represented by *triads* which are connected using *joints*. A joint is used to specify constraints between two triads in a master-slave fashion where the degrees of freedom for the slave joint is dependent on the DOFs of the master triad and the joint specification. In this case a free joint is used, with all of its degrees of freedom fixed except one. A *generic part* is used to connect the two joints, each representing a parallel spring-dashpot connection.

Selecting a rotational degree of freedom to represent the DOFs in the problem is convenient to avoid the static equilibrium to be affected by gravity. The first joint has its master triad attached to ground, whilst inertia for the first mass is introduced to the slave triad. The slave triad is attached to a massless generic part which in turn is attached the master triad for the next joint.

The nonlinear stiffness characteristics describing the backlash is defined as a separate stiffness function with a deadband using polyline function according to table 4.3.

Joint deflection	Stiffness
-0.0501	2000
-0.05	0
0.05	0
0.0501	2000

Table 4.3: Spring characteristics for a spring with $k = 2000 N/m$ and backlash of 0.05 m.

Fedem uses the same family of algorithms for time integration as chosen and formulated in Matlab for this thesis. The Newmark implicit algorithm is explained in section 2.5.2. Fedem however, offers the possibility to include numerical damping without lowering the accuracy through a parameter α (HHT) which is disabled for this comparison. Fedem also uses Newton-Raphson iteration which is described in section 2.5.3, only with a more refined equilibrium convergence criteria

Comparison

A comparison of the solution to the problem stated in figure 4.7 in Fedem and Matlab is first performed by having equal backlash in the two springs.

Mass m_1 [kg]	10
Mass m_2 [kg]	10
Stiffness k_1 [N/m]	2000
Stiffness k_2 [N/m]	2000
Damping c_1 [Ns/m]	0
Damping c_2 [Ns/m]	0
Backlash $b_1/2$ [m]	0.05
Backlash $b_2/2$ [m]	0.05

Table 4.4: System values for comparison of results in Matlab and Fedem
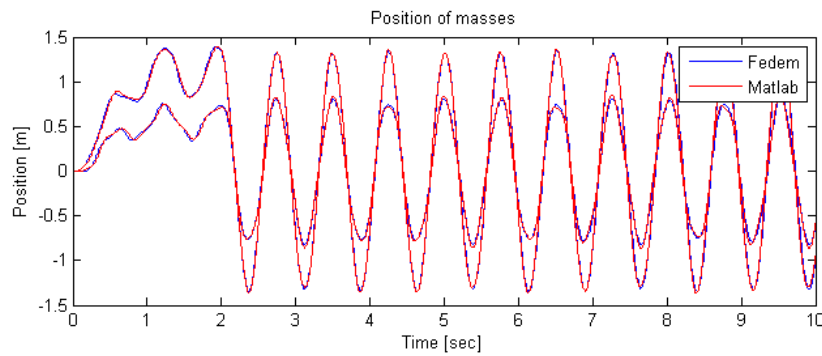

Figure 4.8: Comparison of position of masses for Fedem and Matlab with zero backlash

By introducing backlash and changing the parameters according to table 4.5 the results are compared in figure 4.9.

Mass m_1 [kg]	10
Mass m_2 [kg]	10
Stiffness k_1 [N/m]	2000
Stiffness k_2 [N/m]	1000
Damping c_1 [Ns/m]	0
Damping c_2 [Ns/m]	0
Backlash $b_1/2$ [m]	0.05
Backlash $b_2/2$ [m]	0.03

Table 4.5: System values for comparison of results in Matlab and Fedem with backlash
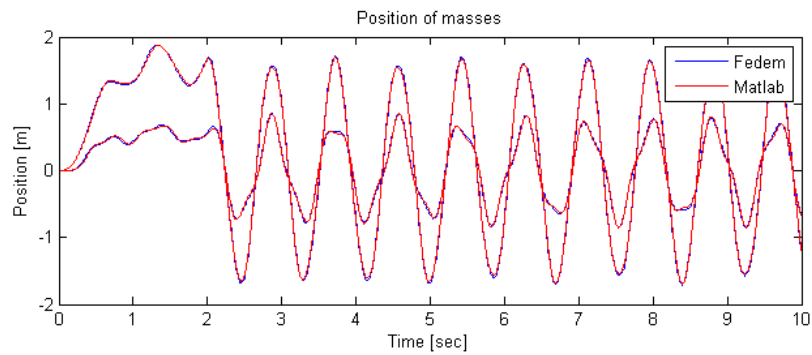
Figure 4.9: Comparison of position of masses for Fedem and Matlab with backlash

As seen in figure 4.8 and 4.9 the two solutions are generally in agreement.

4.5   Combining the camshaft model and gear model

Chapter 5

Results

5.1 Eigenvalue analysis

By neglecting the damping terms in equation 3.3 and assuming the forcing vector is zero, the undamped natural frequencies can be found by solving the eigenvalue problem (equation 2.11). The system is thus symmetrised and the eigenvectors will be real, see section 2.3.3. The undamped natural frequencies are found using both *MATLAB R2015a* and *Abaqus 6.14*.

MATLAB eig()-function uses algorithms either based on *Cholesky decomposition* or *QZ algorithm*, depending on the conditions of the matrices. Refer to MATLAB documentation for details.

In Abaqus the *Subspace iteration algorithm* is used which was developed by Bathe [1] for large structures like buildings and bridges. This method is suitable for structures with many degrees of freedom where only the lowest frequencies and modes are of interest. The camshaft is modelled accurately according to production drawings inertia as described in chapter 3. See figure 3.5.

The frequencies are summarised in the following tables. The mode shapes can be found in appendix A.3.1. The multibody system (MBS) matrices derived in chapter 3 are solved using MATLAB eig()-function and compared with finite element software (FEM) Abaqus.

Mode	MBS [Hz]	FEM [Hz]	Diff. [%]
1	167.10	166.57	0.32
2	412.70	410.23	0.60
3	659.60	658.61	0.15
4	886.00	890.43	-0.50
5	1075.30	1085.60	-0.96

Table 5.1: First five torsional eigenfrequencies of camshaft with 6 cylinder units

Mode	MBS [Hz]	FEM [Hz]	Diff. [%]
1	149.71	147.30	1.61
2	361.48	356.95	1.25
3	584.16	573.81	1.77
4	800.53	782.14	2.30
5	996.76	971.07	2.58

Table 5.2: First five torsional eigenfrequencies of camshaft with 7 cylinder units

Mode	MBS [Hz]	FEM [Hz]	Diff. [%]
1	138.20	136.86	0.97
2	331.56	329.13	0.73
3	535.70	530.64	0.94
4	737.20	730.20	0.95
5	927.68	918.00	1.04

Table 5.3: First five torsional eigenfrequencies of camshaft with 8 cylinder units

Mode	MBS [Hz]	FEM [Hz]	Diff. [%]
1	122.66	120.58	1.70
2	287.15	284.06	1.08
3	461.77	456.11	1.23
4	635.45	626.09	1.47
5	788.97	802.28	1.66

Table 5.4: First five torsional eigenfrequencies of camshaft with 9 cylinder units

5.1.1   Mode shapes

The mode shapes shows the vibration pattern of the camshaft as it resonates at
the different natural frequencies, mode 1 corresponding to the first frequency,
mode 2 to the second frequency etc. The mode shapes for the natural
frequencies are obtained in both Matlab and Abaqus. The first modes for
the 9 cylinder camshaft is presented here. For additional mode shapes, see
appendix A.3.1. The camshaft is shown with its left side being the free end.
Following, in the right end side of the figure is the camshaft extension piece.
The torsional mode shapes in the shaft are displayed by grossly exaggerating
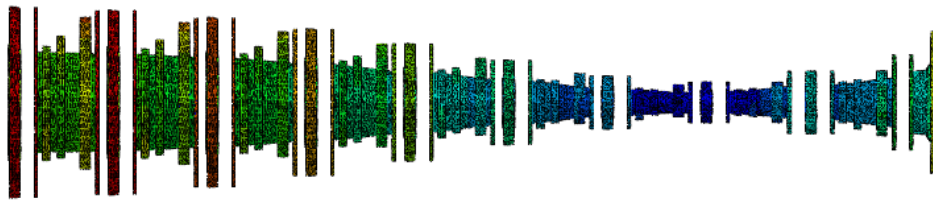the deformation.

Figure 5.1: Fundamental torsional mode for 9 cylinder camshaft using finite
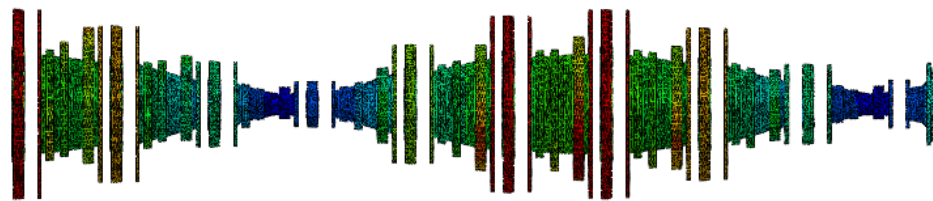element (120.6 Hz)

Figure 5.2: Second normal torsional mode for 9 cylinder camshaft using finite
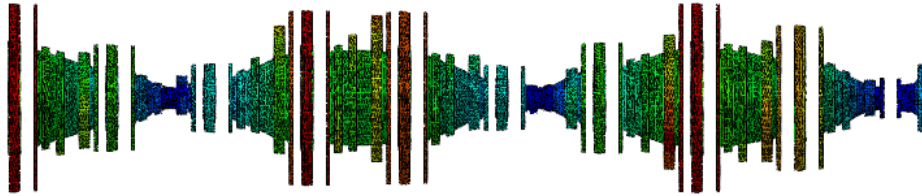element (284.1 Hz)

Figure 5.3: Third torsional normal mode for 9 cylinder camshaft using finite element (456.1 Hz)
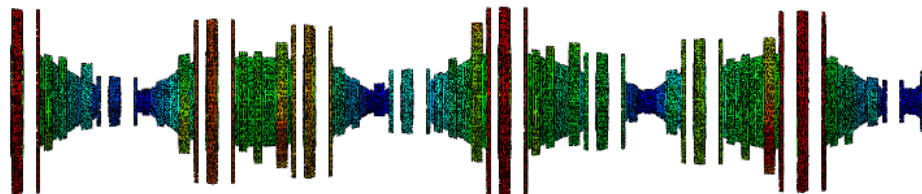

Figure 5.4: Fourth torsional normal mode for 9 cylinder camshaft using finite element (626.1 Hz)

As a comparison, the same mode shapes are obtained in Matlab and plotted as shown in figures below.
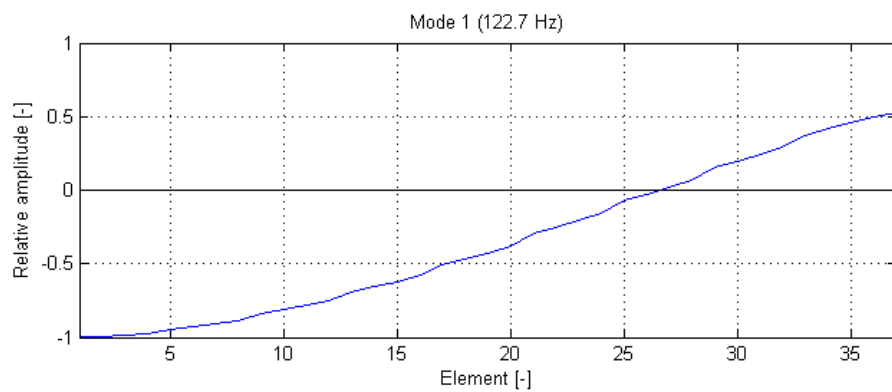

Figure 5.5: Fundamental mode for discrete model of camshaft (9 cyl.)
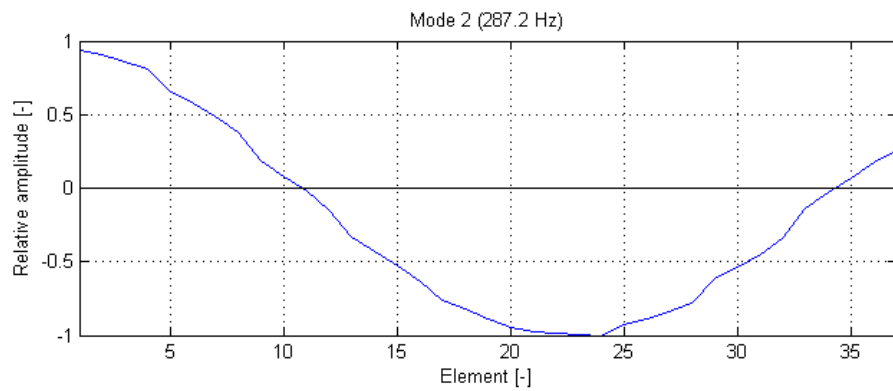
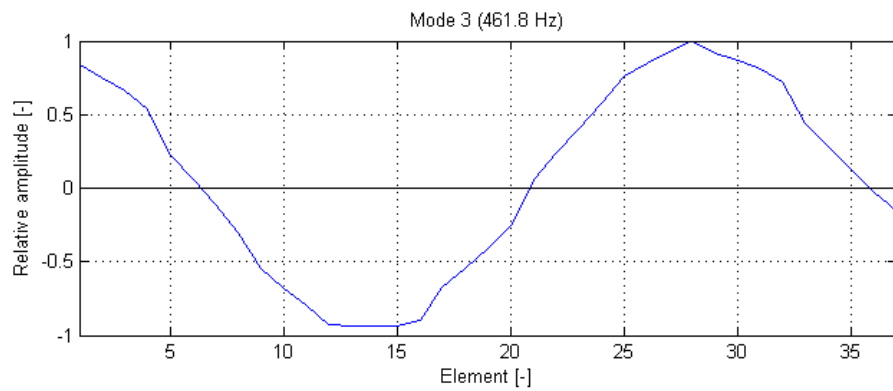Figure 5.6: Second normal mode for discrete model of camshaft (9 cyl.)

Figure 5.7: Third normal mode for discrete model of camshaft (9 cyl.)
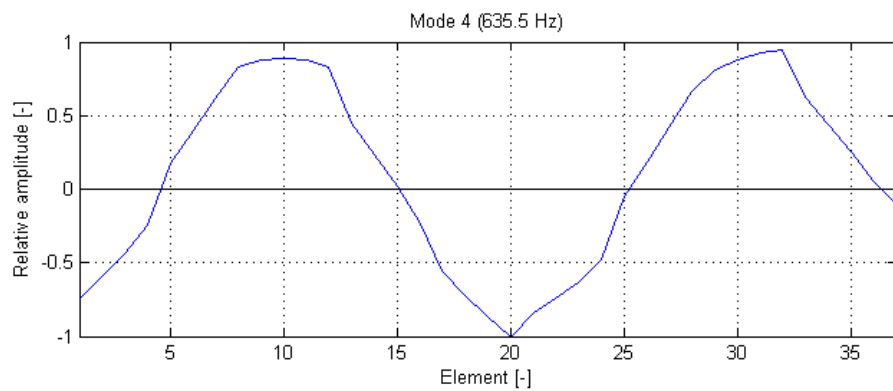

Figure 5.8: Fourth normal mode for discrete model of camshaft (9 cyl.)

5.1.2   Constrained camshaft

The natural frequencies of the system may also be found by introducing a disturbance to the system in equilibrium as described in section 2.3.3. The system will vibrate at its natural frequencies and by converting the time history response to the frequency domain, these frequencies are easily found.

By assuming the gear wheel of the camshaft to be rotating with a constant angular velocity Ω, it is constrained ($\theta_1 = 0$) and the natural frequencies of the camshaft are changed. figs. 5.9 to 5.11 shows the frequencies for the 6, 8 and 9 cylinder camshafts.
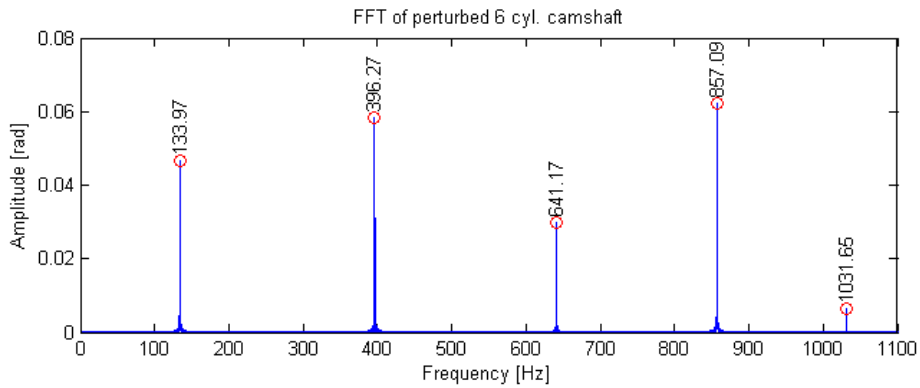

Figure 5.9: Constrained 6 cylinder camshaft natural frequencies
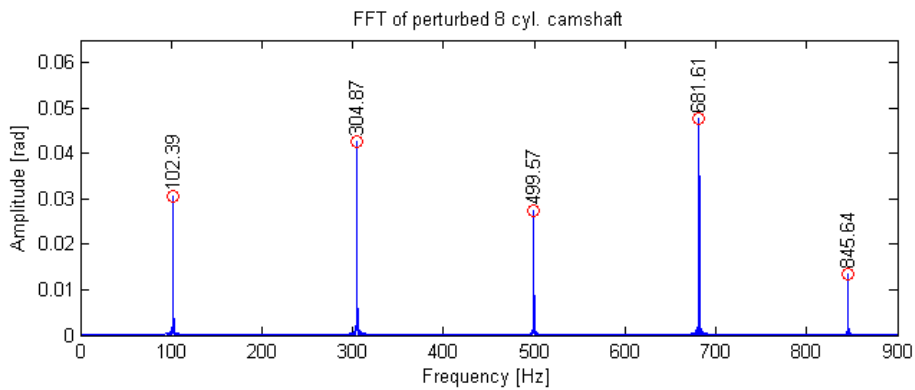

Figure 5.10: Constrained 8 cylinder camshaft natural frequencies
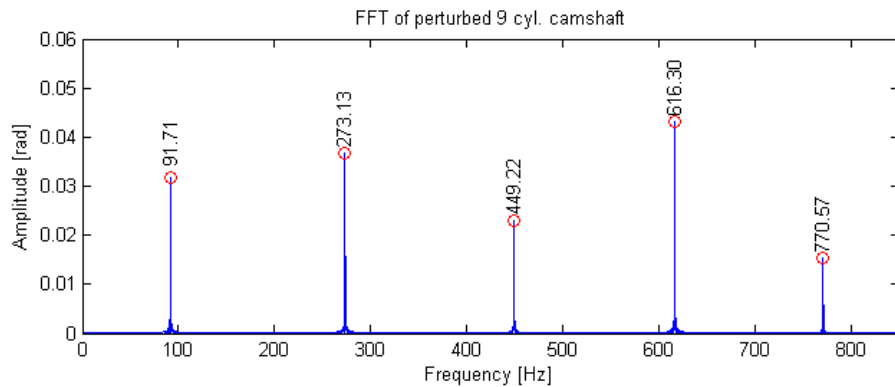
Figure 5.11: Constrained 9 cylinder camshaft natural frequencies

5.2 Transient response of camshaft

In the following sections, the transient and steady state response of the camshaft is presented. For more simulation results, see appendix. The dynamic amplification factor is defined as the maximum torque in the camshaft during the simulation compared to the torque in the static case. By rotating the camshaft at 15 rpm (one revolution every 4th second) the response is taken to be static.

5.2.1 Undamped forced response

The undamped transient response of the camshaft is considered by first neglecting the influences from the crank shaft and gear drive. This means assuming that the camshaft gear wheel rotates with a constant angular velocity; its nominal velocity which is half of the crankshaft speed.

9 cylinders

Number of cylinders	9
Engine speed [rpm]	750
Firing order	1-4-8-2-6-9-3-5-7
Time step [s]	0.001
Number of equilibrium iterations	18937
Simulation period [s]	0-5
Simulation runtime [s]	153
Maximum angular deflection [deg]	1.913
Maximum torque [Nm]	4.721e4
Dynamic amplification factor	3.48

Table 5.5: Simulation summary for 9 cylinder undamped camshaft

Table 5.5 summarises the simulation of the undamped 9 cylinder camshaft for which the response is plotted in the following figure.
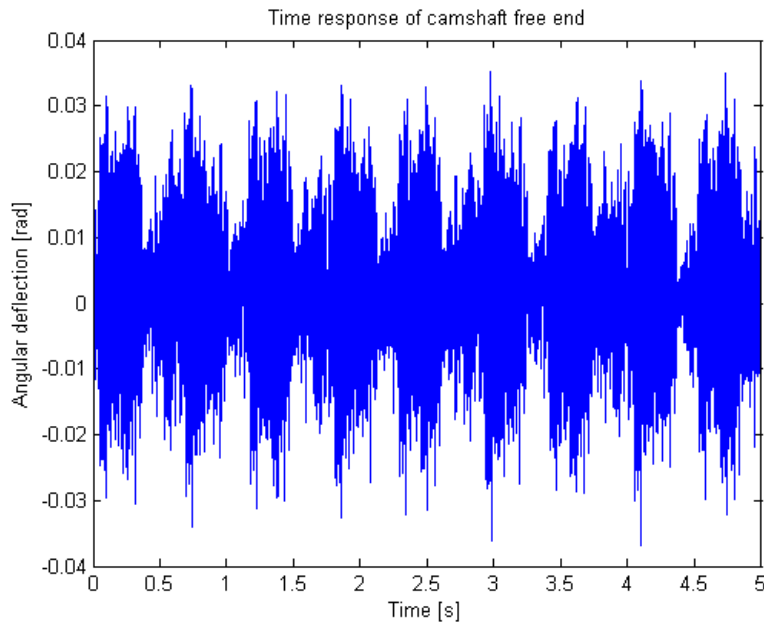
Figure 5.12: Time history response of free end of undamped 9 cylinder camshaft at 375 rpm

By performing a Fast Fourier transformation of the time history response in figure 5.12, the different frequencies are revealed.
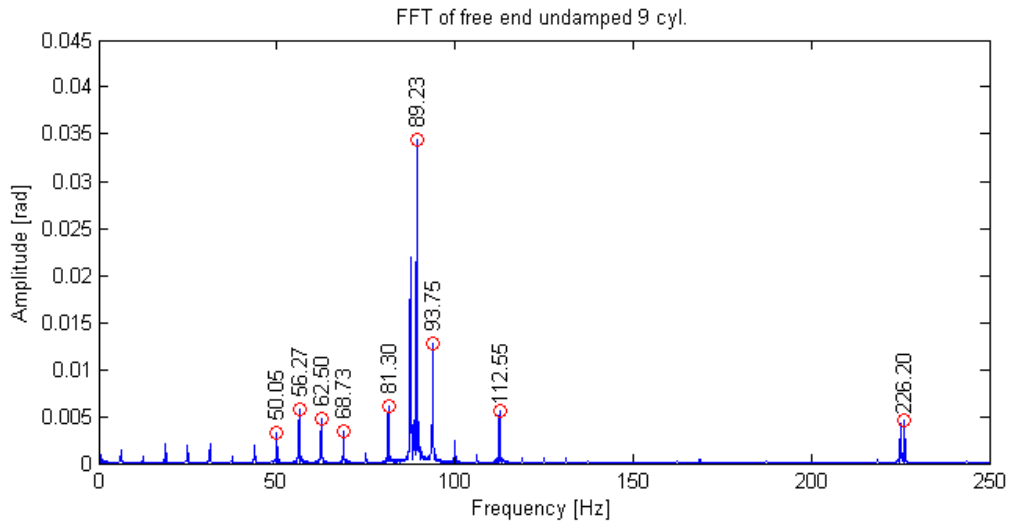
Figure 5.13: Frequency domain response undamped 9 cylinder camshaft (free end)

8 cylinders

Number of cylinders	8
Engine speed [rpm]	750
Firing order	1-8-7-2-6-5-4-3
Time step [s]	0.001
Number of equilibrium iterations	20302
Simulation period [s]	0-5
Simulation runtime [s]	154.6
Maximum angular deflection [deg]	8.623
Maximum torque [Nm]	9.753e4
Dynamic amplification factor	7.34

Table 5.6: Simulation summary for 8 cylinder undamped camshaft
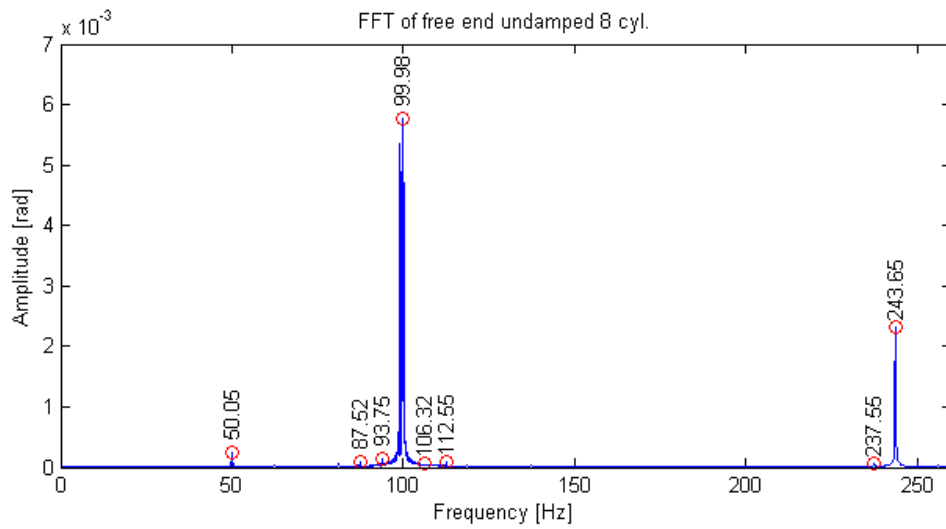
Figure 5.14: Frequency domain response undamped 8 cylinder camshaft (free end)

6 cylinders

Number of cylinders	6
Engine speed [rpm]	750
Firing order	1-5-3-6-2-4
Time step [s]	0.001
Number of equilibrium iterations	17231
Simulation period [s]	0-5
Simulation runtime [s]	101.6
Maximum angular deflection [deg]	0.636
Maximum torque [Nm]	2.139e4
Dynamic amplification factor	1.62

Table 5.7: Simulation summary for 6 cylinder undamped camshaft
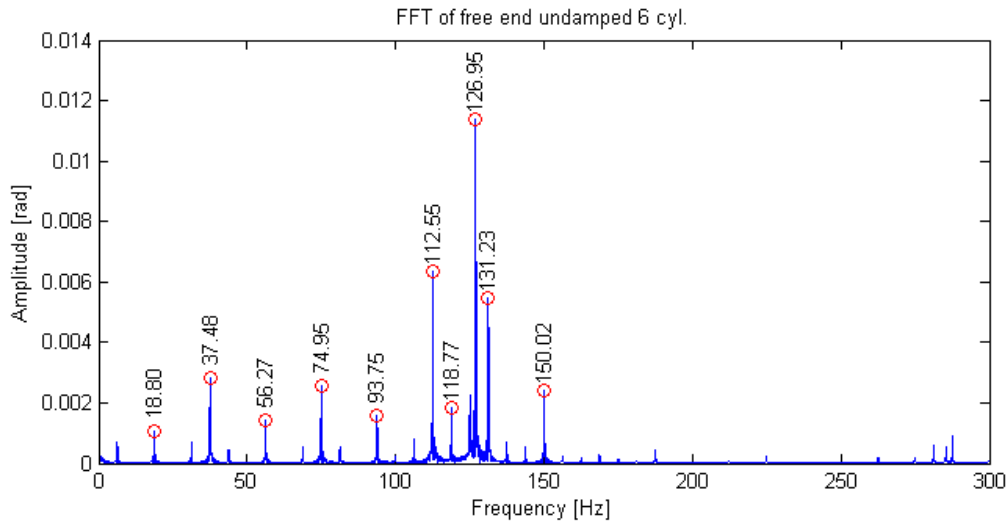
Figure 5.15: Frequency domain response undamped 6 cylinder camshaft (free end)

5.2.2 The effect of damping

Camshaft response is simulated for different values of damping as outlined in section 3.4 and summarized in table 5.2.2.

	Undamped		Case 1		Case 2		Case 3	
	$\Delta\theta$	DAF	$\Delta\theta$	DAF	$\Delta\theta$	DAF	$\Delta\theta$	DAF
6 cyl.	0.636	1.615	0.353	1.196	0.370	1.296	0.360	1.048
8 cyl.	8.623	7.338	2.486	4.786	3.193	5.766	2.131	4.237
9 cyl.	1.913	3.482	0.999	2.437	1.023	2.864	0.946	2.323

Table 5.8: Dynamic amplification factor (DAF) and angular deflection for different damping cases

In the following figures the angular deflection of the camshaft is plotted as the engine speed is slowly increased from 20 to 800 rpm for undamped and three different cases of damping.
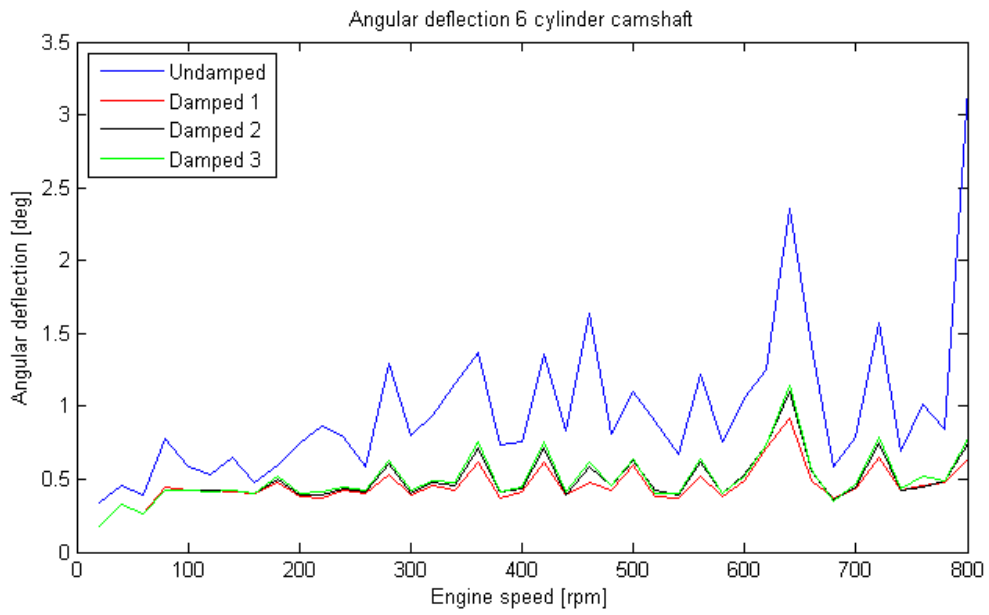
Figure 5.16: Angular deflection of free end during engine startup (6 cyl.)
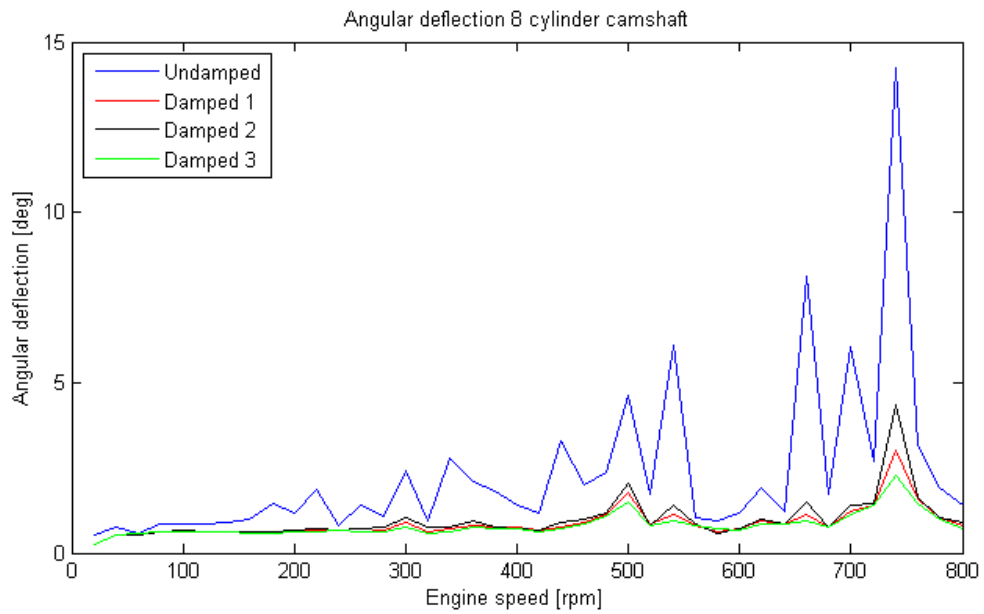
Figure 5.17: Angular deflection of free end during engine startup (8 cyl.)
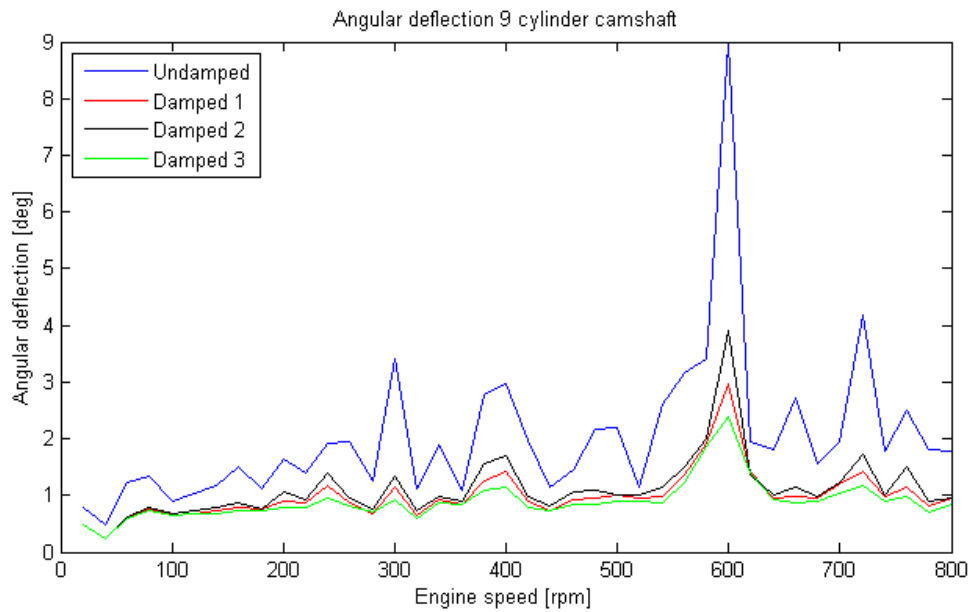
Figure 5.18: Angular deflection of free end during engine startup (9 cyl.)

5.2.3 Effect of engine firing order

The maximum dynamic torque and free end angular deflection is found for a range of firing orders for the 6 and 8 cylinder camshaft,

Firing order	Dynamic Torque	Deflection
	[-]	[deg]
1-5-3-6-2-4	1.787e4	0.366
1-4-3-6-2-5	1.675e4	0.376
1-2-3-4-5-6	2.223e4	0.549
1-6-2-5-3-4	1.862e4	0.488

Table 5.9: Different firing orders for 6 cylinder engine

Firing order	Dynamic Torque	Deflection
	[-]	[deg]
1-8-7-2-6-5-4-3	5.448e4	2.059
1-5-4-8-7-2-6-3	4.772e4	2.043
1-2-7-8-4-5-6-3	5.019e4	2.059
1-5-3-7-4-8-2-6	5.207e4	2.383

Table 5.10: Different firing orders for 8 cylinder engine

5.3 Transient response of camshaft with gear drive

By adding the gear drive and taking the meshing stiffness to be constant average according to table 4.2 undamped response in the 9 cylinder camshaft is simulated and summarised in the following table. For other cylinder configurations, see appendix.

Number of cylinders	9
Engine speed [rpm]	750
Backlash [mm]	0.15 and 0.15
Firing order	1-4-8-2-6-9-3-5-7
Time step [s]	0.001
Number of equilibrium iterations	20977
Simulation period [s]	0-5
Simulation runtime [s]	221.0
Frontside contact [-]	2327
Backside contact [-]	2284
Angular deflection amplitude [deg]	2.602
Dynamic torque amplitude [Nm]	1.847e5

Table 5.11: Simulation summary for 9 cylinder undamped camshaft including gear drive, backlash: 0.15 mm

Number of cylinders	9
Engine speed [rpm]	750
Backlash [mm]	0.15 and 0.15
Firing order	1-4-8-2-6-9-3-5-7
Time step [s]	0.001
Number of equilibrium iterations	21141
Simulation period [s]	0-5
Simulation runtime [s]	229.5
Frontside contact [-]	2139
Backside contact [-]	2049
Angular deflection amplitude [deg]	1.186
Dynamic torque amplitude [Nm]	5.620e4

Table 5.12: Simulation summary for 9 cylinder camshaft-gear, mass proportional damped ($\xi_1 = 0.01$), backlash: 0.15 mm

5.3.1 Effect of gear backlash

Gear backlash is seen to increase the angular deflection of the camshaft as seen in table 5.11. In the follwing table, the effect of gear backlash on angular deflection is further examined

Gear Backlash	Angular amplitude
[mm]	[deg]
0.05	1.092
0.15	1.185
0.25	1.467
0.30	1.838
0.35	1.479
0.43	2.016
0.50	2.411

Table 5.13: Gear backlash effect on camshaft angular amplitude
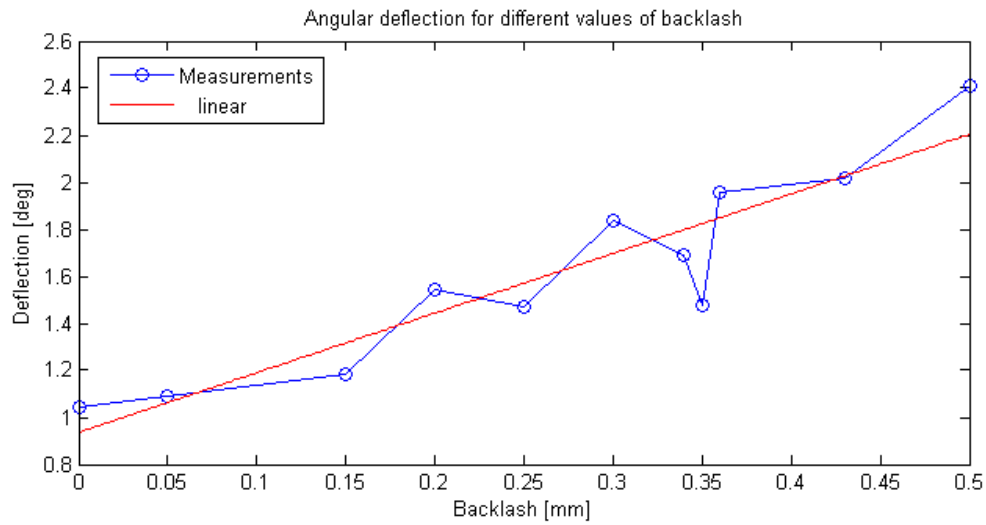
Figure 5.19: Effect of gear backlash on angular deflections in camshaft (damped 8 cyl.)

5.3.2   Effect of time-varying mesh stiffness

A time varying meshing stiffness is calculated using a discontinuous stepping function as described in equation 4.16. The meshing frequencies were $f_{m1} = Z_2\Omega_2$ and $f_{m2} = Z_4\Omega_3$. The two stiffness functions is plotted in the following figure for engine running speed of 750 rpm. The phase difference between the two functions were arbitrarily chosen to be $\psi = \pi/4$
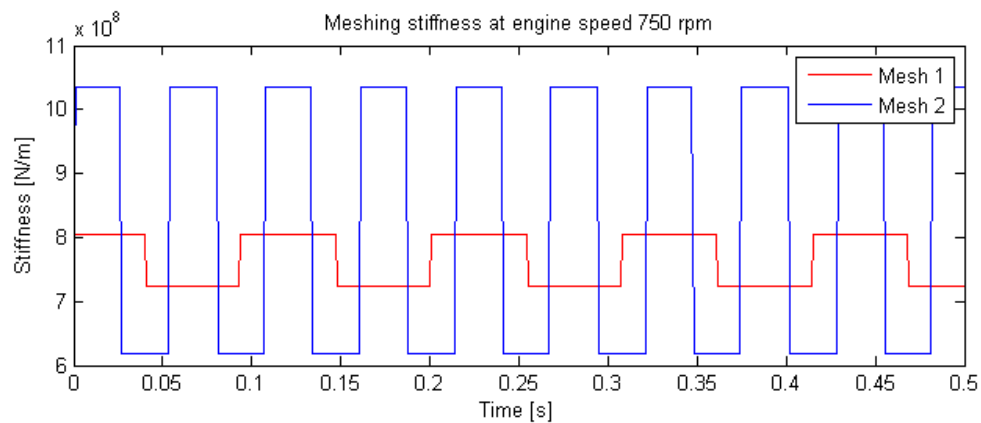
Figure 5.20: Meshing stiffness at engine speed 750 rpm

This is compared with the case where the stiffness was assumed to be constant average

Meshing stiffness [N/m]	Constant average	Time varying
Number of cylinders	9	9
Engine speed [rpm]	750	750
Backlash [mm]	0 and 0	0 and 0
Firing order	1-4-8-2-6-9-3-5-7	1-4-8-2-6-9-3-5-7
Time step [s]	0.001	0.001
Number of equilibrium iterations	14596	14594
Simulation period [s]	0-5	0-5
Simulation runtime [s]	222.0	187.2
Angular deflection amplitude [deg]	1.0433	1.0494
Dynamic torque amplitude [Nm]	1.585e4	1.615e4

Table 5.14: Comparing results for constant average stiffness in meshing gears and time varying stiffness (damping case 1).

Chapter 6

Discussion

6.1 Natural frequencies

The natural frequencies are very important properties of the camshaft as they define the frequencies at which the system will resonate. The undamped natural frequencies are calculated for different cylinder configurations using both finite element software and by solving the eigenvalue problem for the discrete model described in chapter 5.1. The fundamental torsional frequency decreases for increasing number of cylinders on the engine. The differences between the frequencies using the finite element method and the discrete multibody system (MBS) are low, around 1-2 %, see table tables 5.1 to 5.4. This suggests that the spatial discretization of the camshaft is reasonably accurate with respect to the finite element model.

Once the continuous problem is spatially discretized as described in chapter 3, it is thus an efficient way of obtaining the natural frequencies for different cylinder configurations and for tweaking stiffness and mass properties of the system. Solving the eigenvalue problem for the 9 cylinder camshaft took under a second in Matlab and produced about the same results as extracted from the finite element method. As a comparison, the finite element formulation had over 2.8 million degrees of freedom and used almost 4 hours to complete (Intel Core i7 860 @ 2.80GHz).

The frequencies are, however, generally somewhat lower than expected. It is believed that this is partly due to coarse element formulation in Abaqus. The camshaft was modelled with quadratic tetrahedron elements of global size 16 mm. The second order tetrahedral element is generally good for complex geometries, but a coarse mesh will not capture the smaller features of the

solids. For complex geometries a manually meshing technique is often almost impossible, and automatic meshing techniques with tetrahedral elements is less time consuming [3].

Frequencies are also found by perturbing the system from its equilibrium with an initial condition. The resulting motion is converted to the frequency domain using Fast Fourier Transform (FFT). Crucial for the FFT to render higher natural frequencies is to increase the sampling rate, i.e. lowering the time step in the time integration routine. A time step of 0.001 seconds gives a sampling rate of 1000, making the Nyquist limit 500 Hz.

6.2 Transient response of camshaft

Time history response of the camshaft during operation at 750 rpm engine speed shows generally large *angular deflections*. This deflection is an important design parameter in the camshaft design process which directly affects the valve timings. The angular deflection was defined as the difference in angular position between the first and last cam on the shaft. The short duration impulse forces due to the injection pumps are among the sources for transient response in the system, see figure 3.3. Others are the exhaust valve opening and closing, inlet valve opening and closing and various dynamic effects in the valve train, e.g. wind-down.

Each cylinder unit of the shaft have three cams for operating injection pump, exhaust valves and inlet valves. By increasing the number of cylinders, the number of time-varying forces increases. The transient response of camshaft is affected by the firing order of the cylinders mainly due to the forces of the valves alternating between being positive and negative. The effect of different firing orders are however lower than expected. This is due to the short duration injection pump forces being dominant, see figure 3.3.

The camshaft is relatively stiff, and its time history response as shown for the 9 cylinder engine in figure 5.12. The response consists of several frequencies and the figure is hard to read. A Fast Fourier transformation of the time response converts the response into the frequency domain for better readability, see figure 5.13.

The large amplitude of angular deflection and dynamic amplification factor in table 5.6 suggests resonance in the 8 cylinder unit camshaft. At engine operating speed, 750 rpm, the camshaft rotational frequency is 6.25 Hz. Since the fundamental frequency of 102.39 Hz (see figure 5.10) is close to the 16th harmonic of the rotational speed, large amplitudes occur. In general, the

response of all camshafts strongly depend on the fundamental frequencies found in section 5.1 and the frequency of excitation as described in 3.5.

Since the response is dominated by the fundamental frequencies, the influence of damping is also important, as apparent in table 5.2.2. Three cases of damping were found through the assumption of proportional (Rayleigh) damping. In Case 1 the damping was assumed to be purely mass proportional and 1% of critical damping for the first natural frequency. In Case 2 damping was assumed to be stiffness proportional for the same rate ($\xi_1 = 0.01$). In Case 3 a linear combination of both stiffness and mass was assumed by choosing $\xi_1 = 0.01$ and $\xi_2 = 0.02$. Finding realistic values for damping is difficult as described in section 3.4 and should be adjusted by measurements and physical experiments.

Relatively low amplitudes of angular deflection are noted for the 6 cylinder camshaft due to its natural frequencies being far away from the excitation frequencies.

The importance of damping is further illustrated in 5.16. The angular deflection between the first and last cam is shown for different engine running speeds. As the engine speed is increased from static to operation speeds the camshaft is brought through several peaks. This may be due to the duration of the pulses changing with the rotational speed or other oscillating forces from the PLN and valve trains. If there is no damping in the system, these peaks will be large as shown at 600 rpm engine speed for the 9 cylinder camshaft in figure 5.18. In shafts in general it is important for damping to be present if the shaft is brought through critical speeds.

The dynamic amplification factor was defined as the maximum dynamic torque divided by the static torque which was found by rotating the shaft 15 rpm. However, the system experiences some inertial effects even at this slow speed, and the reliability of this factor is reduced.

6.3   Gear backlash

Camshaft dynamic behaviour is examined by including the gear drive dynamics in the equations of motion. The camshaft is powered by the engine crankshaft through a two-stage gear drive with an intermediate idler shaft assumed to be rigid, see chapter 4. The gears was modelled as rigid disks with gear teeth flexibility. The small clearance between the mating gears, backlash, is essential for the gears to operate properly, but introduces complications to the dynamic behaviour of the system.

The gears are designed with profile shift and center distance which gives high contact ratio. This reduces the dynamical contributions to the camshaft performance, but backlash is nonetheless unavoidable.

As seen for the undamped case of 9 cylinder camshaft in table 5.11 the presence of backlash in the two gear stages significantly increases the angular deflection amplitude, even though its defined as the difference in deflection from the first and last cam on the shaft. High dynamic torques is also seen, which could be used for further fatigue studies. The effects of backlash may be overestimated due to low damping.

Gear hammering is seen to occur as the gears alternates between frontside and backside contact which is not desirable as it introduces high impact loads to the gear teeth. Damping is seen to somewhat reduce this effect, see table 5.12. The results are generally in agreement with the expectations, but further studies on the effect of gear backlash needs to be conducted. As shown in figure 5.19, there is a general linear trend but with discrepancies. Further damping may be desirable as it reduces the hammering effect. Attaching a torsional vibration damper which absorbs the accelerations may be an option. Backside contact in high load gears are under normal conditions rare [19], but given the transient vibration after the injection pump impulse loads backside contact is seen to occur very frequently.

The tolerances for backlash in the gears in this study are defined according to the industry standard DIN 3967. Its lower limit is 0.15 mm and upper limit 0.43 mm. As seen in figure 5.19, even small amounts of backlash leads to dynamic contributions to the camshaft, and care should be taken to ensure that the backlash in a gear pair does not exceed the limit. During operation, wear may increase the total backlash over time and readjustments of the gear may be applicable.

6.4 Gear meshing stiffness

Camshaft performance was tested with both constant average gear meshing stiffness and a time-varying stiffness. The stiffness was assumed to alternate between the case single tooth contact and double tooth contact. The parametric excitations in the gears due to this meshing stiffness variation were seen to be insignificant for the systems performance at 750 rpm engine speed. One can expect even lower contributions as the real contact ratios in the gear drive are higher.

6.5 Numerical procedures

To solve the system of nonlinear equations of motion direct integration methods is used. A procedure for numerically solving the differential equations in the time domain is introduced. The method is based on the Newmark-algorithms with constant average acceleration and Newton-Raphson iterations for ensuring equilibrium. By assuming the acceleration over each time step to be constant average, the routine becomes unconditionally stable for linear problems, i.e. the step size can be modified for the desirable accuracy of the solution. Implicit methods were found to be superior to explicit methods due to the stability restrictions in the explicit methods.

For the camshaft time history simulations the time steps were generally chosen to be 0.001 which for the 0-5 second simulation time required about 150 seconds to calculate. Since the external forces were functions of the angular position of the camshaft the equations becomes nonlinear. Newton-Raphson iterations were performed until the equilibrium tolerances were satisfied and only residual force vector was used as iteration criteria. The maximum unbalance (residual) force was set to be 0.001N and 3-4 iteration steps were necessary each time step. This is, however, a stringent criteria and may be reduced to decrease computational costs.

By adding the gear model to the system of equations, solving becomes more time consuming. The strong nonlinearity introduced by the backlash lead to as many as 12 iterations to satisfy the iteration tolerances, see table 5.12. The numerical procedures can be expanded to more accurately simulate the gear behaviour and gear profile errors etc. by e.g. including a more sophisticated contact algorithm to verify the contact forces and to include rigid body kinematics [33]. Numerical damping may also be applicable to stabilise the nonlinear problem without the loss of accuracy, e.g. using the Hilbert-Hughes-Taylor α-method [8].

The calculations were performed in MATLAB environment which is a high-level programming language. Due to its high level, the code is easy to read and maintain, but slower than lower level languages like C and Fortran [28]. Performance can thus be increased by translating the code into lower level languages.

6.6 Validating the results

The results presented in chapter 5 are generally in agreement with the expectations. However, the results are not regarded very reliable until they

are confirmed through physical testing and validating.

Chapter 7

Conclusion

The dynamical behaviour of a medium speed marine engine camshaft is investigated. Special attention is paid to the torsional vibrations.

The camshaft natural frequencies are lowered as the number of cylinder units increases. The dynamical behaviour of the camshafts is found to be dominated by the first natural frequencies and the high impulse loads introduced by the injection pump.

One of the most important design criteria in camshaft design is the angular deflection which influences the valve timing and hence the engine performance. Large amplitudes of angular deflection are found in the camshafts when the forcing frequency is close to one of the natural frequencies and care should be taken to prevent this.

Gear backlash is seen to significantly increase the angular deflection in the camshaft, but is suppressed by damping. A torsional vibration damper may thus be applicable. Stringent tolerances for backlash are also important as the total backlash may be increased by gear wear.

The results obtained were generally in concurrence with the expectations. However, a complete and accurate dynamical model to simulate the complex camshaft response is an extensive task and this thesis only scratches the surface. The results obtained should be validated and tweaked with physical testing for further parameter studies. Unfortunately, the physical measurements were not available in time for the results to be validated. Thus, few definite conclusions can be drawn.

Validation of results and numerical procedures in general remains for further work. A more sophisticated model of the gear dynamics is also desirable

to study parametric instabilities in detail. A coupled torsional and lateral vibration model may be applicable to fully understand the camshaft behaviour.

Bibliography

[1] Klaus-Jürgen Bathe and Edward L. Wilson. Solution methods for eigenvalue problems in structural mechanics. *International Journal for Numerical Methods in Engineering Vol. 6, Issue 2 p 213-226*, 1973.

[2] I. Chowdhury and S.P. Dasgupta. Computation of rayleigh damping coefficients for large systems. *Electron. J. Geotech. Eng. vol 8, pp 1-11*, 2003.

[3] A.O. Cifuentes and A. Kalbag. A performance study of tetrahedral and hexahedral elements in 3-d finite element structure analysis. *Finite Elements in Analysis and Design 12 pp 313-318*, 1992.

[4] James W. Cooley and John W. Tukey. An algorithm for the machine calculation of complex fourier series. *Mathematics of Computation, Vol. 19, No. 90, pp 297-301*, 1965.

[5] DIN. Calculation of load capacity of cylindrical gears; introduction and general influence factors. Technical report, Deutsches Institut für Normung e.V., 1987.

[6] DIN. Din 867:1986-02 basic rack tooth profiles for involute teeth of cylindrical gears for general engineering and heavy engineering. Technical report, Deutsches Institut für Normung, Geneva, Switzerland, 1998.

[7] Paolo L. Gatti. *Applied Structural and Mechanical Vibrations Theory and Methods, 2nd ed.* CRC Press, 2014.

[8] M. Géradin and D. Rixen. *Mechanical Vibrations - Theory and Application to Structural Dynamics 2nd ed.* John Wiley & Sons Inc., 1997.

[9] S. L. Harris. Dynamic loads on the teeth of spur gears. *Proceedings of the Institution of Mechanical Engineers 172,87-112*, 1958.

[10] T. E. Hull, W. E. Enright, B. M. Fellen, and A. E. Sedgwick. Comparing numerical methods for ordinary differential equations. *SIAM Journal Numerical analysis vol.9 No. 4*, 1972.

[11] ISO. Iso 53:1998(e) cylindrical gears for general and heavy engineering - standard basic rack tooth profile 2nd ed. Technical report, International Organization for Standardization, Geneva, Switzerland, 1998.

[12] ISO. Iso 6336-1:2006 calculation of load capacity of spur and helical gears. Technical report, International Organization for Standardization, Geneva, Switzerland, 2006.

[13] Damir T. Jelaska. *Gears and Gear Drives*. John Wiley & Sons Inc., 2012.

[14] A.J. Jerri. The shannon sampling theorem—its various extensions and applications: A tutorial review. *Proceedings of the IEEE vol. 65, issue 111, pp 1565-1596*, 1992.

[15] A. Kahraman and G. W. Blankenship. Effect of involute contact ratio on spur gear dynamics. *Journal of Mechanical Design 121(1), 112-118*, 1999.

[16] M. Kushawaha, H. Rahnejat, and Z.M. Jin. Valve-train dynamics: A simplified triboelasto-multi-body analysis. *Proceedings of the Institution of Mechanical Engineers, Part K: Journal of Multi-body Dynamics, vol. 214, no. 2, pp. 95-110*, 2000.

[17] Prem K. Kythe and Dongming Wei. An introduction to linear and nonlinear finite element analysis, 2004.

[18] H.H. Ling and R. Huston. Dynamic loading on parallel shaft gears. *NASA Contractor Report 179473*, 1986.

[19] G. Liu and R. G. Parker. Nonlinear, parametrically excited dynamics of two-stage spur gear trains with mesh stiffness fluctuation. *Proceedings of the Institution of Mechanical Engineers, Part C: Journal of Mechanical Engineering Science*.

[20] W.K. Liu and T. Belytschko. Mixed-time implicit-explicit finite elements for transient analysis. *Journal of Applied Mechanics 45:445-450*, 1982.

[21] R. G. Munro. Dynamic behaviour of spur gears. *Ph.D. Dissertation, Cambridge University*, 1962.

[22] B.L. Newkirk. Shaft whipping. *General Electric Review*, 1924.

[23] Nathan M. Newmark. A method of computation for structural dynamics. *Journal of the Engineering Mechanics Division of ASCE Vol. 85, No. 3, July 1959, pp. 67-94*, 1959.

[24] H. Opitz. Dynamic behaviour of spur and helical gears. *Proceedings of the Japanese Society of Mechanical Engineers Semi-International Gearing Symposium 199-209*, 1967.

[25] K. O. Friedrichs R. Courant and H. Lewy. Üeber die partiellen differenzengleichungen der mathematischen physik. *Mathematische Annalen 100, 32-74.*, 1928.

[26] Stephen P. Radzevich. *Dudley's Handbook of Practical Gear Design and Manufacture 2nd ed.* CRC Press, 2012.

[27] DR. Gonzalo González Rey. Higher contact rations for quieter gears. *Gearssolutions.com*, January 2009.

[28] S. B. Sheppard, B.Curtis, P. Milliman, and T. Love. Modern coding practices and programmer performance. *IEEE Computer 5, pp. 41-49*, 1979.

[29] Simula. Abaqus 6.13 user manual. `http://ivt-abaqusdoc.ivt.ntnu.no:2080/v6.13/`,.

[30] Simula. Abaqus 6.13 user manual. http://ivt-abaqusdoc.ivt.ntnu.no:2080/v6.13/.

[31] M. Teodorescu, M. Kushawaha, H. Rahnejat, and D. Taraza. Elasto-dynamic transient analysis of a four-cylinder valvetrain system with camshaft flexibility. *Proceedings of the Institution of Mechanical Engineers, Multi-body Dynamics vol 219, pp 13-25*, 2005.

[32] K. Umezawa, T. Sato, and J. Ishikawa. Simulation on rotational vibration of spur gears. *The Japan Society of Mechanical Engineers, 27(223) 102-109*, 1984.

[33] P. Velex and M-Maatar. A mathematical model for analysing the influence of shape deviations and mounting errors on gear dynamic behaviour. *Journal of Sound and Vibration 191(5) pp.629-660*, 1996.

[34] J. Wang and I. Howard. The torsional stiffness of involute spur gears. *Proceedings of the Institution of Mechanical Engineers, Part C: Journal of Mechanical Engineering Science January 1, vol. 218 no. 1 131-142*, 2004.

[35] K. L. Wang and H. S. Cheng. A numerical solution to the dynamic load, film thickness, and surface temperatures in spur gears, part i: Analysis. *Journal of Mechanical Design, 103(1) p 177-187*, 1981.

[36] T. Yamamoto. *Linear and nonlinear rotordynamics: A modern treatment with applications.* John Wiley & Sons Inc., 2001.

[37] H. Nevzat Özgüven and D.R. Houser. Mathematical models used in gear dynamics - a review. *Journal of Sound and Vibration 121(3), 383-411,* 1988.

Appendix A

Appendix

A.1 Python code

A.1.1 MacroReadDataLine.py

```python
##-------------
from abaqus import*
from part import *
from assembly import *
from interaction import *
from job import *
from sketch import *
from abaqusConstants import*

# Startup

gModel = mdb.Model("Gear Model");
gPart = gModel.Part(name="GearPart", dimensionality=TWO_D_PLANAR,
type=DEFORMABLE_BODY);
#For 3d solid part, set dimensionality=THREE_D

gSketch = gModel.ConstrainedSketch(name = "Sketch A", sheetSize=1000);
myDataLinesS = 0;
coordinateList = [];

# Retrieve data from text file
inputFile = open('Line.txt');
inputFileData = inputFile.readlines();
```

```python
# Read coordinates from text
for i in range(0, len(inputFileData)-1) :
    streng = inputFileData[i];
    x = float(streng.split('\t')[0]);
    y = float(streng.split('\t')[1]);
    coordinateList.append((x,y));

gSketch.Line(point1=(0,0), point2=coordinateList[0]);
gSketch.Spline(points=coordinateList);

# If sketch needs to be closed manually
#gSketch.Line(point1=coordinateList[len(coordinateList)-1], point2=(0,0));

gPart.BaseShell(sketch = gSketch);
# For 3d solid part change to(set depth to tooth face width)
# gPart.BaseSolidExtrude(sketch=gSketch, depth=20.0)

viewPort = session.Viewport(name='Gear',origin=(10, 10),
width=150, height=100);

viewPort.setValues(displayedObject=gPart);

viewPort.partDisplay.setValues(renderStyle=SHADED);
```

A.2   Matlab routines

A.2.1   TimeStepping.m

```matlab
%% Time stepping
i=1;
tc = ti+h0;
h = h0;
while tc+h < tf
    t(i+1) = t(i)+h;

    %% Update camshaft nominal position and rotational speed
    position(i+1) = position(i) ...
        + speed(i)/60*360 * h;
    if mod(i,10) == 2
        speed(i+1) = speed(i) + (RPM-RPM_start)*h;
    else
        speed(i+1) = speed(i);
    end
```

```matlab
%% Expand matrices if necessary
if i+1 > nSteps
    T = [T zeros(nDofs,1)];
    u = [u zeros(nDofs,1)];
    ud = [ud zeros(nDofs,1)];
    udd = [udd zeros(nDofs,1)];
end

%% Predict solutions
ud(:,i+1) = ud(:,i) + (1-gamma)*h*udd(:,i);
u(:,i+1) = u(:,i) + h*ud(:,i)+(0.5-beta)*h*h*udd(:,i);
udd(:,i+1) = 0;

%% Update external force vector
torque = zeros(nDofs,1);
for k=0:N_cyl-1;
    angle = position(i+1) + PHASE_ANGLES(k+1);
    torque(4*k+3) = interp1(FUEL_X,FUEL_Y,rem(angle+...
        u(4*k+3,i+1),360),'linear');
    torque(4*k+4) = interp1(EXHAUST_X,EXHAUST_Y,rem(angle+...
        u(4*k+4,i+1),360), 'linear');
    torque(4*k+5) = interp1(INLET_X,INLET_Y,rem(angle+...
        u(4*k+5,i+1),360), 'linear');
    torque(4*k+6) = 0;
end
T(:,i+1) = torque;

%% Check residual force vector
r = M*udd(:,i+1) + K_t*u(:,i+1) + C_t*ud(:,i+1) - T(:,i+1);

%% Iterate towards equilibrium
j = 0;
while (max(abs(r)) > iterationCriteria) && (j <= maxIterationSteps)
    %% Update tangent stiffness matrix
    K_t = K; %Linear
    C_t = C; %Linear

    %% Update external force vector
    torque = zeros(nDofs,1);
    for k=0:N_cyl-1;
        angle = position(i+1) + PHASE_ANGLES(k+1);
        torque(4*k+3) = interp1(FUEL_X,FUEL_Y,rem(angle+...
            u(4*k+3,i+1),360), 'linear');
        torque(4*k+4) = interp1(EXHAUST_X,EXHAUST_Y,rem(angle+...
```

```
                u(4*k+4,i+1),360), 'linear');
            torque(4*k+5) = interp1(INLET_X,INLET_Y,rem(angle+...
                u(4*k+5,i+1),360), 'linear');
            torque(4*k+6) = 0;
         end
         T(:,i+1) = torque;

         %% Calculate the Jacobian matrix
         J = K_t + gamma/(beta*h)*C_t + 1/(beta*h*h)*M;

         %% Boundary Conditions ( First mass station attatched to ground)
         J(:,1) = 0;
         J(1,:) = 0;
         J(1,1) = 1;
         r(1) = 0;

         du = J \ -r;

         %% Correction
         u(:,i+1) = u(:,i+1) + du;
         ud(:,i+1) = ud(:,i+1) + gamma/(beta*h)*du;
         udd(:,i+1) = udd(:,i+1) + 1/(beta*h*h)*du;

         %% New residual
         r = M*udd(:,i+1) + K_t*u(:,i+1) + ...
             C_t*ud(:,i+1) - T(:,i+1);
         j = j + 1;
    end

    %% Abort if convergence is not found
    if j > maxIterationSteps
        fprintf('Max number of iterations reached for step %d\n', i);
        break;
    end

    tc = t(i);
    i = i + 1;
end
```

A.2.2 CheckContact.m

```
function [G,W] = CheckContact(u1,u2,bl)
% Checks for contact conditions in connection with backlash
    delta = u2-u1;
```

```matlab
    if delta > bl                              % Driven-side contact
        G = 1;
        W = -bl;
    elseif delta < -bl                         % Backside contact
        G = 1;
        W = bl;
    else                                       % Contact loss
        G = 1e-20;
        W = 1e-20;
    end
end
```

A.2.3 FFT.m

```matlab
function FFT (t_vec,y_vec,limit)
% Generates a frequency spectrum plot from 0 Hz to limit Hz.
    Fs = 1/(t_vec(1,2) - t_vec(1,1));          % Sampling frequency
    N = length(t_vec);                         % Sampling points

    NFFT = 2^nextpow2(N);
    y = fft(y_vec,NFFT) /Fs;
    f = Fs/2*linspace(0,1,NFFT/2+1);

    frequency = f(1:NFFT/2);
    amplitude = abs(y(1:NFFT/2));

    [pks,locs] = findpeaks(amplitude,...        % Locate peaks
                        'SortStr','descend',...
                        'MinPeakDistance',50,...
                        'Npeaks',10);

    xLocs = frequency(locs);

    plot(frequency,amplitude,xLocs,pks,'or');
    for i=1:length(xLocs)
        h = text(xLocs(i), pks(i), sprintf(' %6.2f', xLocs(i)));
        set(h,'Rotation',90);
    end

    title('FFT');
    xlim([0 limit]);
end
```

A.2.4   GenerateStiffnessMatrix.m

```
function K = GenerateStiffnessMatrix ( m_vec )
% Generates a tridiagonal stiffness matrix from a vector of stiffnesses
    N = length(m_vec);
    K = zeros(N,N);

    K(1,1) = k_vec(1);
    K(1,2) = - k_vec(1);
    for i = 2:N-1;
        K(i,i-1) = -k_vec(i-1);
        K(i,i) = k_vec(i-1) + k_vec(i);
        K(i,i+1) = -k_vec(i);
    end
    K(N,N-1) = -k_vec(N-1);
    K(N,N) = k_vec(N-1);

end
```

A.2.5   GenerateMassMatrix.m

```
function M = GenerateMassMatrix ( m_vec )
% Generates a diagonal mass matrix
    N = length(m_vec);
    M = zeros(N,N);

    for i = 1:N;
        M(i,i) = m_vec(i);
    end

end
```

A.3 Results

A.3.1 Eigenvalue analysis

6 cylinder units
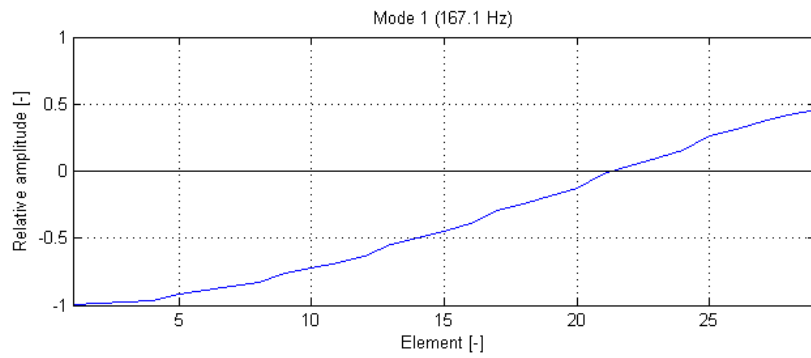
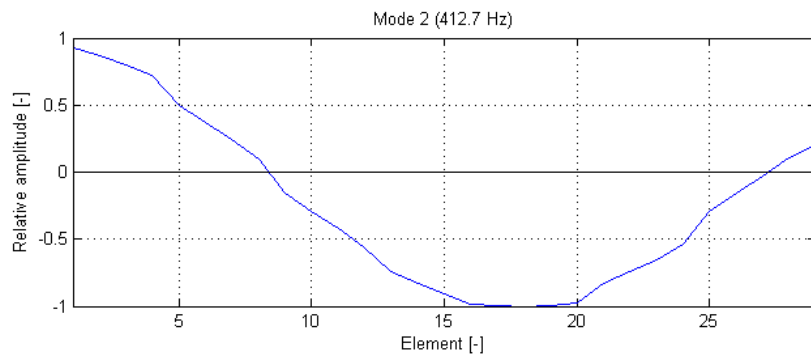Figure A.1: Fundamental mode for discrete model of camshaft (6 cyl.)

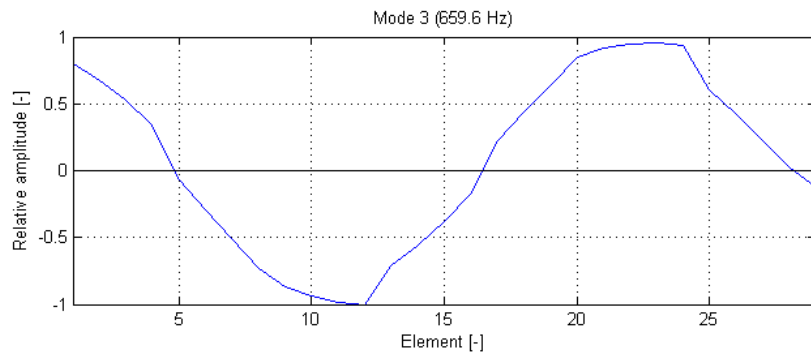Figure A.2: Second normal mode for discrete model of camshaft (6 cyl.)

Figure A.3: Third normal mode for discrete model of camshaft (6 cyl.)
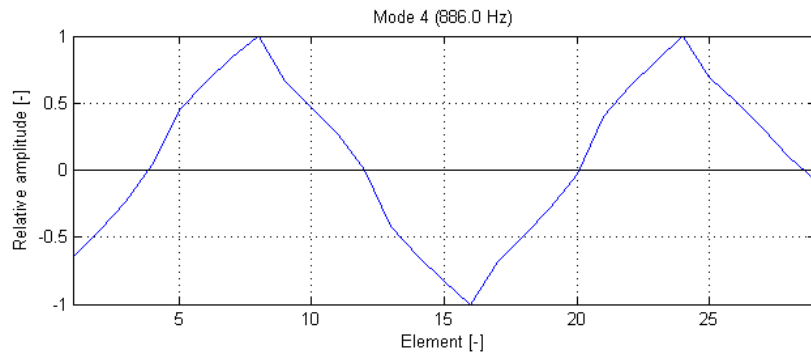

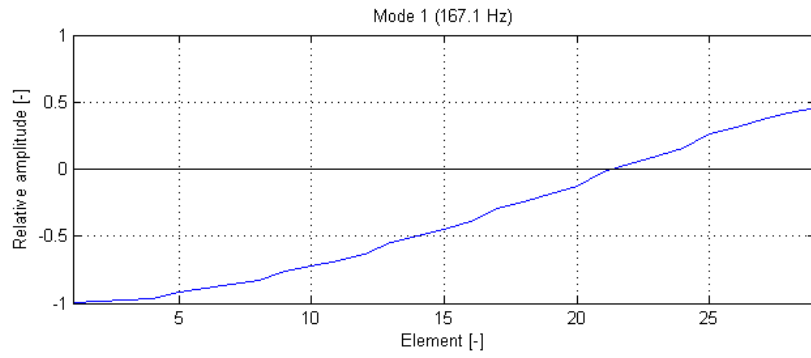Figure A.4: Fourth normal mode for discrete model of camshaft (6 cyl.)

8 cylinder units

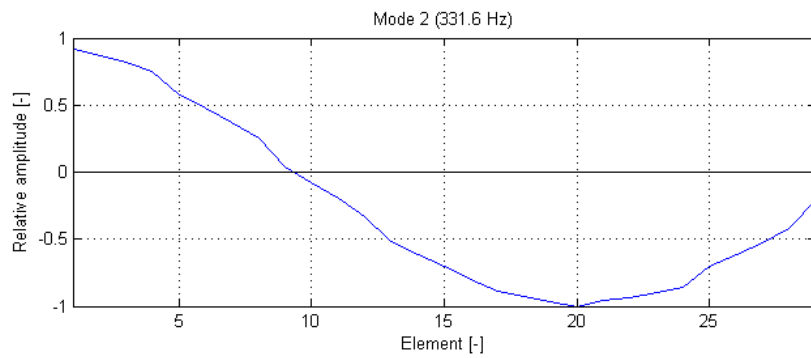Figure A.5: Fundamental mode for discrete model of camshaft (6 cyl.)

Figure A.6: Second normal mode for discrete model of camshaft (8 cyl.)
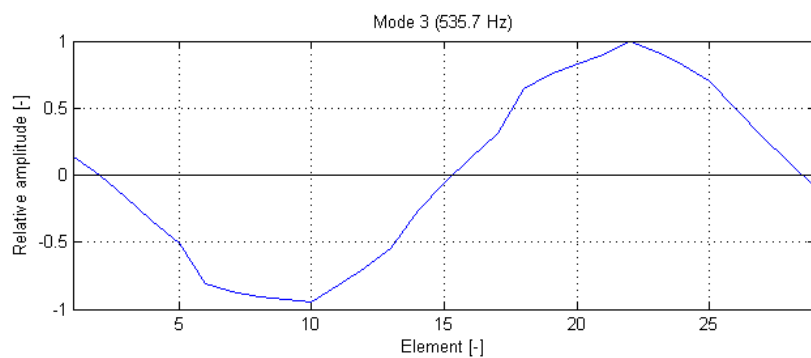

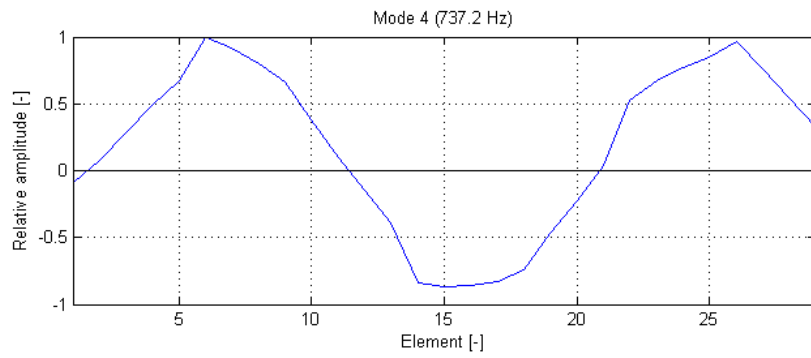Figure A.7: Third normal mode for discrete model of camshaft (8 cyl.)

Figure A.8: Fourth normal mode for discrete model of camshaft (8 cyl.)
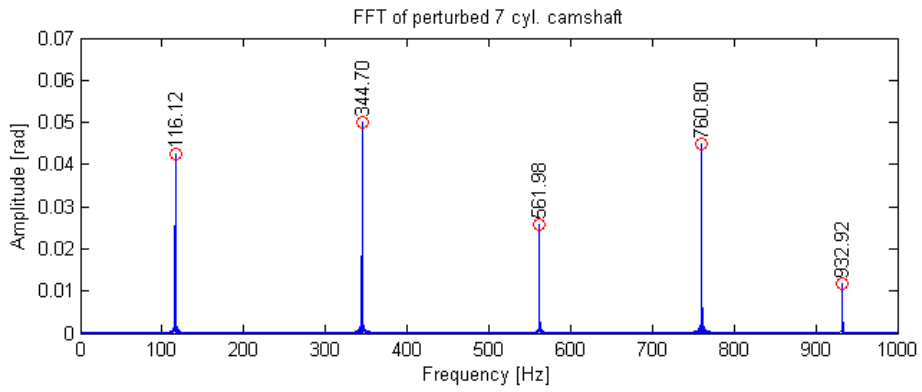

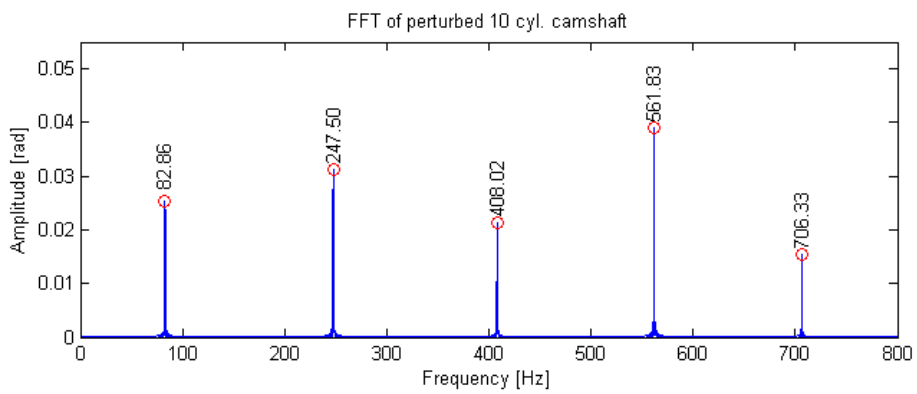Figure A.9: Constrained 7 cylinder camshaft natural frequencies

Figure A.10: Constrained 10 cylinder camshaft natural frequencies

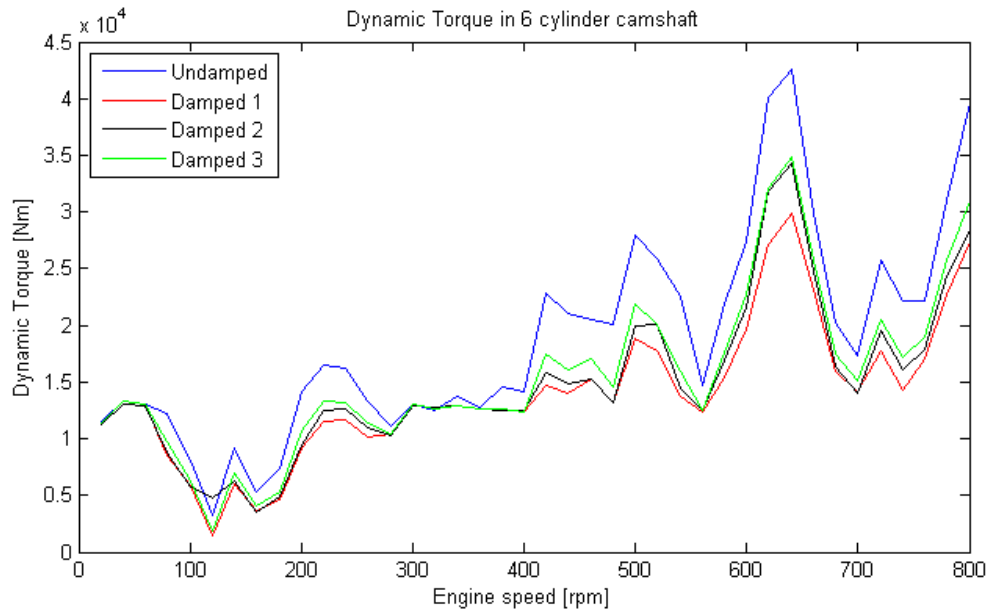## A.3.2 Transient response

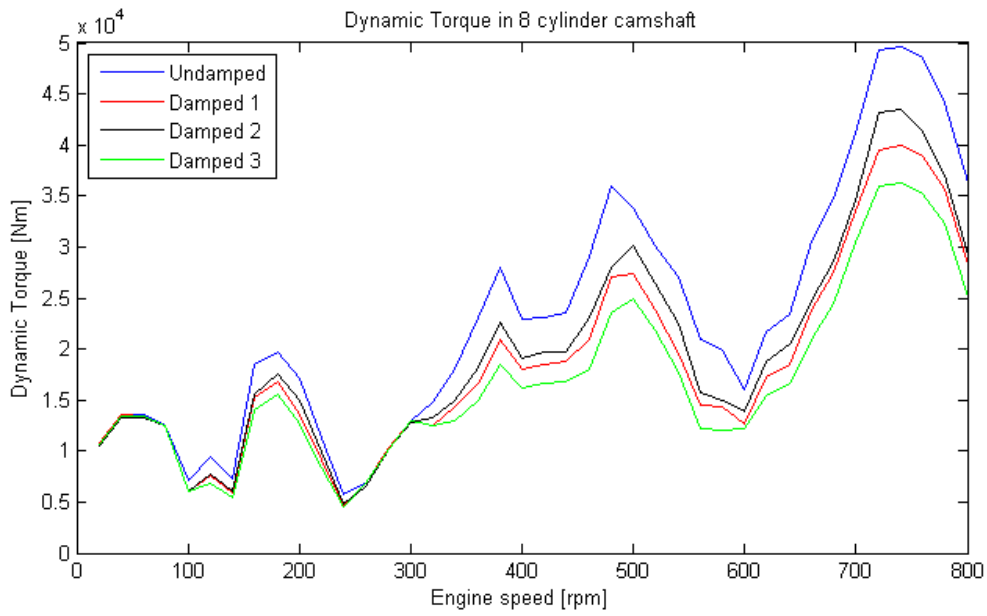Figure A.11: Maximum dynamic torque in camshaft during startup (6 cyl.)

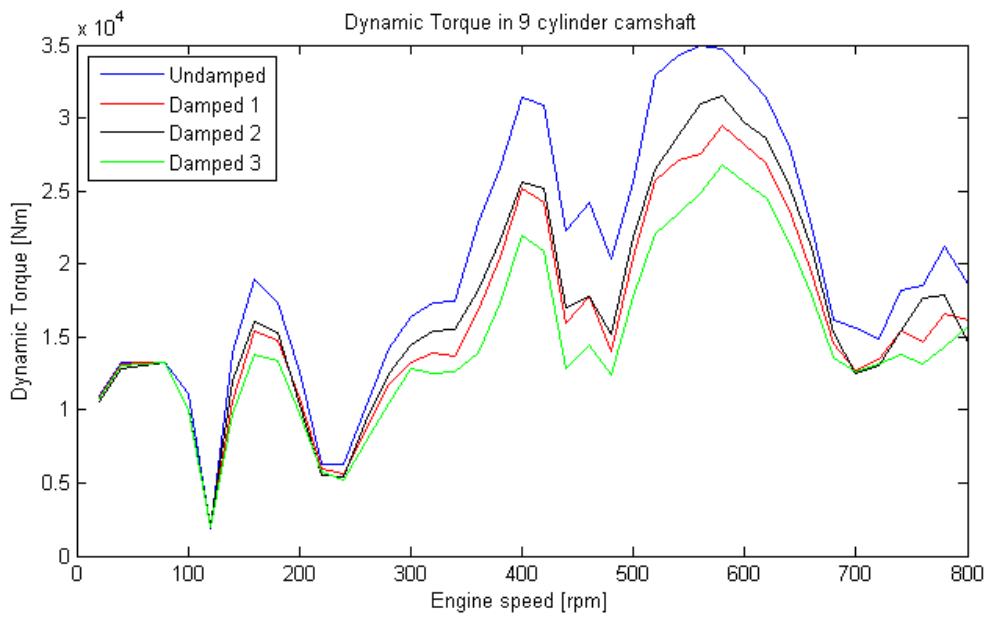Figure A.12: Maximum dynamic torque in camshaft during startup (8 cyl.)

Figure A.13: Maximum dynamic torque in camshaft during startup (9 cyl.)

NTNU		
🔘		
HMS		

	Utarbeidet av	Nummer	Dato
	HMS-avd.	HMSRV2601	22.03.2011
	Godkjent av		Erstatter
	Rektor		01.12.2006

Kartlegging av risikofylt aktivitet

Enhet: **IPM**   **Dato: 14.01.2015**

Linjeleder: Torgeir Welo

Deltakere ved kartleggingen (m/ funksjon):
(Ansv. veileder, student, evt. medveiledere, evt. andre m. kompetanse)

Kort beskrivelse av hovedaktivitet/hovedprosess: Masteroppgave, Steffen Loen Sunde - Mekanisk analyse av kamaksel på skipsmotor

Er oppgaven rent teoretisk? (JA/NEI):   **JA**   *«JA» betyr at veileder innestår for at oppgaven ikke inneholder noen aktiviteter som krever risikovurdering.   Dersom «JA»: Beskriv kort aktiviteten i kartleggingskjemaet under. Risikovurdering trenger ikke å fylles ut.*

Signaturer: *Ansvarlig veileder:* Bjørn Haugen   *Student:* Steffen L. Sunde

ID nr.	Aktivitet/prosess	Ansvarlig	Eksisterende dokumentasjon	Eksisterende sikringstiltak	Lov, forskrift o.l.	Kommentar
1	Litteraturstudie, dataassisterte beregninger	Steffen				
2	Rapportskriving	Steffen				

NTNU

	Utarbeidet av	Nummer	Dato
	HMS-avd.	HMSRV2601	22.03.2011
	Godkjent av		Erstatter
HMS	Rektor		01.12.2006

Risikovurdering

Enhet:

Linjeleder:

Deltakere ved kartleggingen (m/ funksjon):
(Ansv. Veileder, student, evt. medveiledere, evt. andre m. kompetanse)

Risikovurderingen gjelder hovedaktivitet: Masteroppgave student xx. Tittel på oppgaven.

Signaturer: *Ansvarlig veileder:* *Student:*

Dato:

ID nr	Aktivitet fra kartleggings-skjemaet	Mulig uønsket hendelse/belastning	Vurdering av sannsyn-lighet (1-5)	Vurdering av konsekvens:				Risiko-Verdi (menn-eske)	Kommentarer/status Forslag til tiltak
				Menneske (A-E)	Ytre miljø (A-E)	Øk/materiell (A-E)	Om-dømme (A-E)		

Risikovurdering

Sannsynlighet vurderes etter følgende kriterier:

Svært liten 1	Liten 2	Middels 3	Stor 4	Svært stor 5
1 gang pr 50 år eller sjeldnere	1 gang pr 10 år eller sjeldnere	1 gang pr år eller sjeldnere	1 gang pr måned eller sjeldnere	Skjer ukentlig

Konsekvens vurderes etter følgende kriterier:

Gradering	Menneske	Ytre miljø Vann, jord og luft	Øk/materiell	Omdømme
E Svært Alvorlig	Død	Svært langvarig og ikke reversibel skade	Drifts- eller aktivitetsstans >1 år.	Troverdighet og respekt betydelig og varig svekket
D Alvorlig	Alvorlig personskade. Mulig uførhet.	Langvarig skade. Lang restitusjonstid	Driftsstans > ½ år Aktivitetsstans i opp til 1 år	Troverdighet og respekt betydelig svekket
C Moderat	Alvorlig personskade.	Mindre skade og lang restitusjonstid	Drifts- eller aktivitetsstans < 1 mnd	Troverdighet og respekt svekket
B Liten	Skade som krever medisinsk behandling	Mindre skade og kort restitusjonstid	Drifts- eller aktivitetsstans < 1uke	Negativ påvirkning på troverdighet og respekt
A Svært liten	Skade som krever førstehjelp	Ubetydelig skade og kort restitusjonstid	Drifts- eller aktivitetsstans < 1dag	Liten påvirkning på troverdighet og respekt

Risikoverdi = Sannsynlighet x Konsekvens
Beregn risikoverdi for Menneske. Enheten vurderer selv om de i tillegg vil beregne risikoverdi for Ytre miljø, Økonomi/materiell og Omdømme. I så fall beregnes disse hver for seg.

Til kolonnen "Kommentarer/status, forslag til forebyggende og korrigerende tiltak":
Tiltak kan påvirke både sannsynlighet og konsekvens. Prioriter tiltak som kan forhindre at hendelsen inntreffer, dvs. sannsynlighetsreduserende tiltak foran skjerpet beredskap, dvs. konsekvensreduserende tiltak.

Risikomatrise

MATRISE FOR RISIKOVURDERINGER ved NTNU

KONSEKVENS			SANNSYNLIGHET		
	Svært liten	**Liten**	**Middels**	**Stor**	**Svært stor**
Svært alvorlig	E1	E2	E3	E4	E5
Alvorlig	D1	D2	D3	D4	D5
Moderat	C1	C2	C3	C4	C5
Liten	B1	B2	B3	B4	B5
Svært liten	A1	A2	A3	A4	A5

Prinsipp over akseptkriterium. Forklaring av fargene som er brukt i risikomatrisen.

Farge	Beskrivelse
Rød	Uakseptabel risiko. Tiltak skal gjennomføres for å redusere risikoen.
Gul	Vurderingsområde. Tiltak skal vurderes.
Grønn	Akseptabel risiko. Tiltak kan vurderes ut fra andre hensyn.